Ore Geology Reviews 65 (2015) 1110–1126

Contents lists available at ScienceDirect

Ore Geology Reviews

journal homepage: www.elsevier.com/locate/oregeorev

Boron isotopic constraints on the Nb and Ta mineralization of the syenitic dikes in the ~260 Ma Emeishan large igneous province (SW China)

Fen-Lian Wang [a,b], Christina Yan Wang [a], Tai-Ping Zhao [a,*]

[a] Key Laboratory of Mineralogy and Metallogeny, Guangzhou Institute of Geochemistry, Chinese Academy of Sciences, Guangzhou 510640, China
[b] University of Chinese Academy of Sciences, Beijing 100039, China

ARTICLE INFO

Article history:
Received 12 June 2014
Received in revised form 6 September 2014
Accepted 8 September 2014
Available online 16 September 2014

Keywords:
B and B isotope
Nb–Ta mineralization
Syenitic dike
Panxi region
Emeishan large igneous province

ABSTRACT

Both Nb–Ta-mineralized and Nb–Ta-poor syenitic dikes in the Panxi region (SW China) are spatially and temporally associated with syenitic plutons, which are part of the ~260 Ma Emeishan large igneous province. These syenitic dikes are NW-striking, and have width varying from 1 to 5 m and length from 50 to 300 m. The dikes are mainly composed of K-feldspar, albite, aegirine and arfvedsonite, however, mineral modes are different in the Nb–Ta-mineralized and Nb–Ta-poor syenitic dikes. The major Nb–Ta-bearing mineral in the dikes is pyrochlore, which is closely associated with albite and occurs in places with intensive albitization. Rocks of the Nb–Ta-mineralized syenitic dikes contain more albite and less K-feldspar than the Nb–Ta-poor dikes, and have compositions more evolved than the Nb–Ta-poor dikes, indicating that the Nb–Ta-mineralized syenitic dikes formed from a highly evolved magma. We analyzed the B concentrations and B isotopic compositions of the samples of both Nb–Ta-mineralized and Nb–Ta-poor syenitic dikes and associated syenitic pluton using a single column purification method and ICP-AES and MC-ICP-MS techniques. The samples of the Nb–Ta-mineralized syenitic dikes have whole-rock B concentrations ranging from 11.4 to 23.9 ppm and $\delta^{11}B$ values from −17.95 to −14.54‰, whereas the samples of the Nb–Ta-poor dikes and syenitic plutons have B concentrations varying from 3.32 to 16.5 ppm and $\delta^{11}B$ values from −13.45 to −10.02‰. The high B concentration of the Nb–Ta-mineralized dikes relative to the Nb–Ta-poor dikes is consistent with that B is incompatible and tends to be rich in more evolved magma. The relatively low $\delta^{11}B$ values of the Nb–Ta-mineralized dikes indicate that the B isotopes may have fractionated between fluids and rocks in a transitional, magmatic–hydrothermal stage. We propose that the highly evolved magmas in a transitional, magmatic–hydrothermal stage may have Nb– and Ta–fluorine complexes dissolved in the hydrothermal fluids in the presence of Na^+. Albite crystallization due to intensive albitization in this stage resulted in the decrease of Na^+ in the fluids, decomposing the Nb– and Ta–fluorine complexes. The released Nb and Ta from the complexes were then dissolved in the fluids and finally entered the lattice of pyrochlore crystals in the stage of albitization.

1. Introduction

The ~260 Ma Emeishan large igneous province (LIP) in SW China consists of massive flood basalts and associated mafic–ultramafic intrusions and felsic plutons (Chung and Jahn, 1995; (Shellnutt and Zhou, 2007; Xu et al., 2001; Zhou et al., 2002a, 2002b). Giant Fe–Ti oxide deposits and economic Ni–Cu–(PGE) sulfide deposits are hosted in some of the mafic–ultramafic intrusions (Wang and Zhou, 2006; Wang et al., 2010; Zhong et al., 2011; Zhou et al., 2005, 2008), whereas Nb and Ta mineralization is hosted in syenitic dikes in the Panzhihua–Xichang (Panxi) region, central part of the Emeishan LIP. The Nb–Ta-mineralized syenitic dikes in the Panxi region are spatially associated with the granitic and syenitic plutons and the mafic–ultramafic layered intrusions of the Emeishan LIP (Fig. 1). These syenitic dikes are recently dated to be ~258 Ma by LA–ICP-MS zircon U–Pb dating technique (Wang et al., 2013), indicating that they are also part of the Emeishan LIP.

High field strength element (HFSE)-rich peralkaline granites commonly occur as small-scaled dikes, sills or plugs and are considered to have formed from highly fractionated and volatile-rich magmas (Boily and Williams-Jones, 1994; Hadj-Kaddour et al., 1998; Kovalenko et al., 1995). As HFSE-rich peralkaline granites experienced remarkably hydrothermal overprints, the high concentrations of rare earth elements (REE) and HFSE in the rocks are attributed to the remobilization of these elements in hydrothermal fluids (Beus et al., 1962; Kempe et al., 1999). Nb–Ta-mineralized syenitic dikes have been reported in the Panxi region since 1960s (He, 2004), however, such an occurrence of Nb–Ta mineralization is rare in the LIPs elsewhere (Li et al., 2012; Xiao

* Corresponding author.
E-mail address: tpzhao@gig.ac.cn (T.-P. Zhao).

http://dx.doi.org/10.1016/j.oregeorev.2014.09.009
0169-1368/

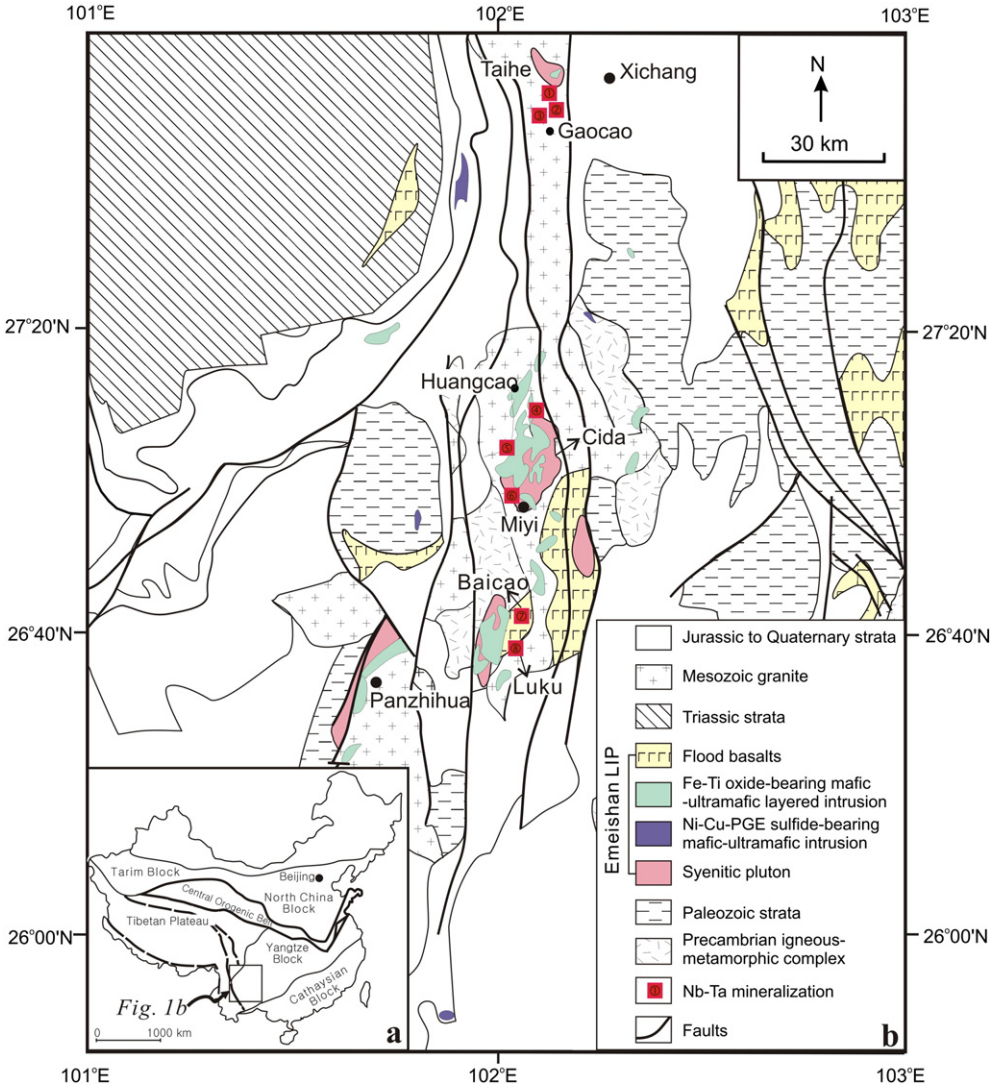

Fig. 1. A geological map of the Panxi region showing the distribution of the flood basalts, mafic–ultramafic intrusions, granitic and syenitic plutons and syenitic dikes and associated Nb–Ta mineralization in the Emeishan large igneous province.
After He (2004), Pang et al. (2009) and Xing et al. (2012).

et al., 2007). It remains unknown whether there is a genetic link between hydrothermal fluids and Nb and Ta enrichment in these syenitic dikes.

Boron is highly soluble in fluids (Barth, 1993). It is highly mobile in a large range of temperature from magmatic to hydrothermal processes and is independent of the oxidation–reduction status of magmas and hydrothermal fluids (Leeman and Sisson, 1996; Slack, 1996). Its stable isotopes, ^{10}B and ^{11}B, can be highly fractionated in fluids due to mass differences (Barth, 1993). Therefore, B is widely used as a sensitive tracer to examine fluid–rock interaction and hydrothermal processes in the formation of hydrothermal ore deposits (Deyhlea and Kop, 2005; Jiang et al., 1998, 1999; Leeman and Sisson, 1996; Palmer and Swihart, 1996; Palmer and Slack, 1989; Slack et al., 1993).

In this study, we present the whole-rock major and trace element compositions, and B concentrations and B isotopic compositions of the Nb–Ta-mineralized and Nb–Ta poor syenitic dikes and associated syenitic plutons in the Panxi region. The new data set enables us to examine magma evolution and the role of hydrothermal overprint on the enrichment of Nb and Ta in these syenitic dikes.

2. Geological background

In SW China, the Yangtze Block is bounded by the Tibetan Plateau to the west, and the Indochina Block to the south. The Yangtze Block has a Mesoproterozoic basement overlain by Neoproterozoic to Cenozoic cover (Yan et al., 2003). The volcanic succession of the Emeishan LIP in SW China varies in thickness from several hundred meters to ~5 km and is mainly composed of low-Ti and high-Ti flood basalts (Chung and Jahn, 1995; Xu et al., 2001). There are also numerous coeval mafic–ultramafic intrusions and granitic and syenitic plutons (Shellnutt and Iizuka, 2012; Zhou et al., 2008). The Emeishan LIP is believed to have been formed from a mantle plume at ~260 Ma (Chung and Jahn, 1995).

In the Panxi region, the flood basalts of the Emeishan LIP crop out over a wide area (Fig. 1b). Several NS-trending faults have exposed spatially associated mafic–ultramafic intrusions and granitic and syenitic plutons of the Emeishan LIP. The Fe–Ti oxide-bearing, mafic–ultramafic layered intrusions constitute a mineralized belt about 300 km long and 10 to 30 km wide, forming the most important metallogenic region for

Fe, Ti and V in China (Ma et al., 2003; Zhou et al., 2005). The Fe–Ti oxide-bearing, layered intrusions in the Panxi region intruded the Sinian Dengying Formation composed of limestone, or locally intruded the Emeishan flood basalts (Zhong et al., 2003; Zhou et al., 2002a). Small mafic–ultramafic intrusions that emplaced Devonian and Carboniferous strata may host Ni–Cu–(PGE) sulfide deposits. Felsic plutons have compositions varying from peralkaline, metaluminous and peraluminous (Shellnutt and Zhou, 2007; Shellnutt et al., 2008, 2009a, 2009b; Xu et al., 2008; Zhong et al., 2007, 2009).

More than 30 small Nb–Ta deposits in the Panxi region are reported and most of them are hosted in syenitic dikes (He, 2004), among which the two largest ones are the Luku and Baicao mines (Fig. 1). The reserve of the Luku mine is estimated to be 465 tons of Nb_2O_5 and 30 tons of Ta_2O_5 (unpublished report of the No. 403 geological team in the Sichuan Bureau of Geology, 1965). In this study, the syenitic dikes that contain >150 ppm Nb and >10 ppm Ta are denoted as Nb–Ta-mineralized dikes, whereas those with <150 ppm Nb and <10 ppm Ta are denoted as Nb–Ta-poor dikes.

In the Luku mine, the syenitic pluton is covered by the interlayers of sandstone and mudstone of the Neogene Xigeda Formation and intruded the limestone of the Sinian Dengying Formation. Syenitic dikes occur to the east of the syenitic pluton (Fig. 2) and intruded the mafic–ultramafic layered intrusion (Fig. 4a and b). Most dikes are orientated along a NW strike. Some of these dikes are Nb–Ta-mineralized, whereas the others are Nb–Ta-poor dikes. The Nb–Ta-poor syenitic dikes occur closer to the syenitic pluton than the Nb–Ta-mineralized dikes. The Nb–Ta-mineralized syenitic dikes are 0.5 to 30 m wide and 50 to 300 m long, whereas the Nb–Ta-poor dikes are 1 to 20 m wide and 50 to 400 m long. Aegirine veinlet occurs along the long axis in some Nb–Ta-mineralized syenitic dikes (Fig. 4c), which is rarely observed in the Nb–Ta-poor dikes.

The Baicao mine is 5 km away to the northeast of the Luku mine. Syenitic dikes in this mine occur to the east of the syenitic pluton and also intruded the mafic–ultramafic layered intrusion (Fig. 3). Nb–Ta-mineralized syenitic dikes are dendritic-like or lens-like about 10 to 775 m long and 1 to 5 m wide, whereas those Nb–Ta-poor dikes are 20 to 150 m long and <6 m wide (unpublished report of the Xichang geological team in the Sichuan Bureau of Geology, 1962). All the dikes in the Baicao mine have similar orientation as those in the Luku mine. Some dikes are Nb–Ta-mineralized syenitic dikes, whereas the others not. Like those in the Luku mine, the Nb–Ta-poor syenitic dikes are closer to the syenitic pluton (Fig. 3).

3. Petrography

The Nb–Ta-mineralized and Nb–Ta-poor syenitic dikes in the Luku and Baicao mines have similar mineral assemblages. However, the Nb–Ta-mineralized syenitic dikes are commonly pegmatitic in grain size and have fine- to medium-grained minerals in local places, whereas the Nb–Ta-poor syenitic dikes are mainly composed of fine- to medium-

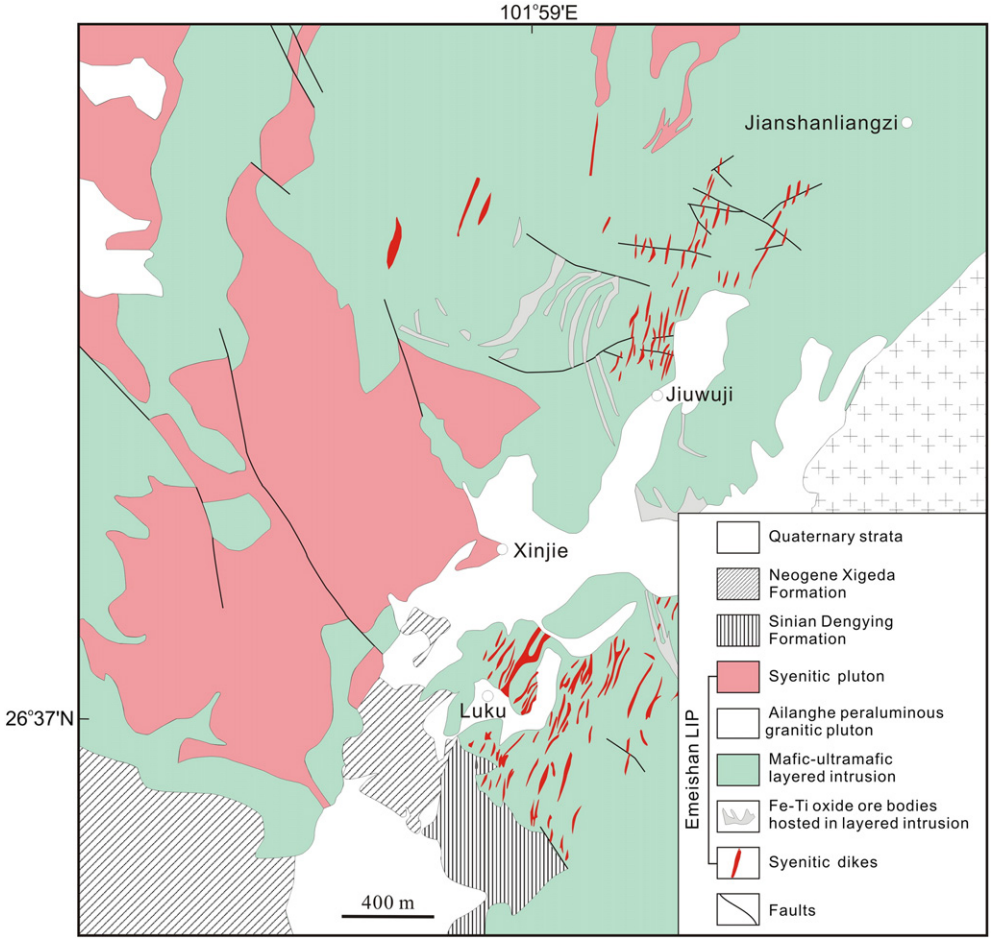

Fig. 2. A geological map showing the relationship of syenitic dikes, mafic–ultramafic layered intrusion and syenitic pluton in the Luku mine. After No.403 Geological Team in the Sichuan Bureau of Geology (1965).

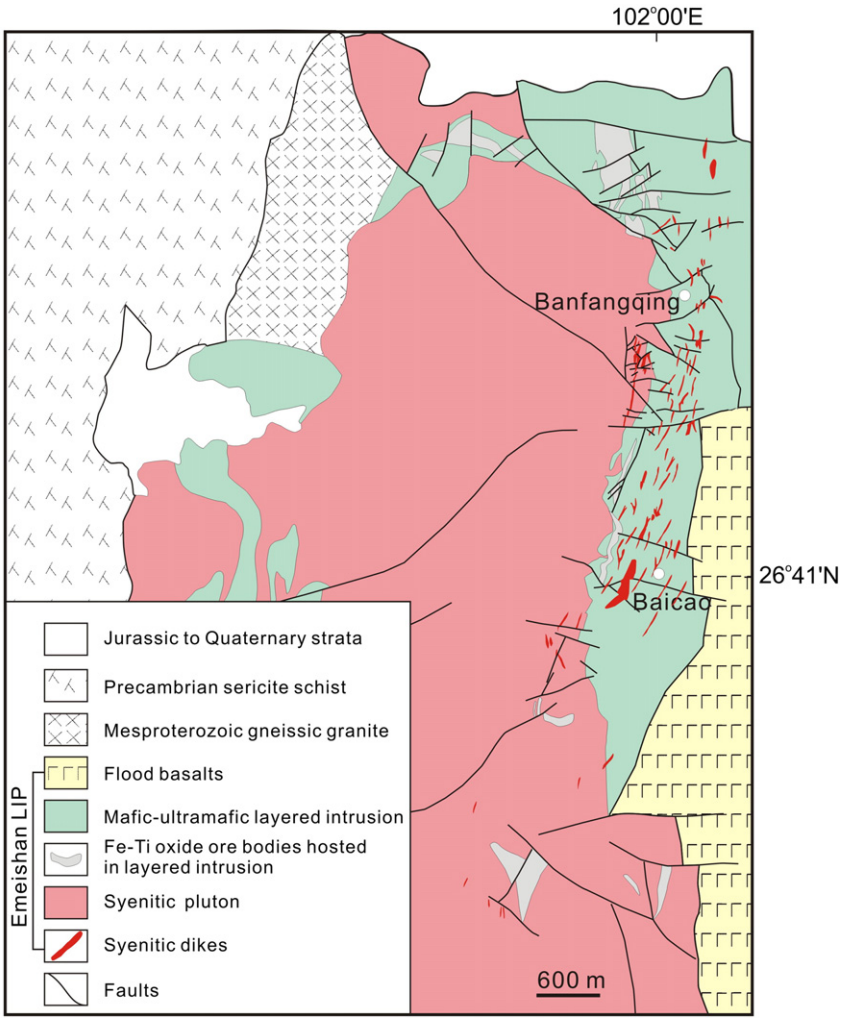

Fig. 3. A geological map showing the relationship of syenitic dikes, mafic–ultramafic layered intrusion and syenitic pluton in the Baicao mine. After the Xichang Geological Team in the Sichuan Bureau of Geology (1962).

grained minerals with pegmatitic minerals in local places. In addition, the Nb–Ta-mineralized syenitic dikes experienced more intensive albitization than the Nb–Ta-poor syenitic dikes.

3.1. Nb–Ta-mineralized syenitic dikes

Rocks of the Nb–Ta-mineralized syenitic dikes are mainly composed of K-feldspar (30–50 modal%, mainly perthite and microcline), albite (10–30%), aegirine (5–15%), arfvedsonite (5–10%) and biotite (1–2%). Perthite, microcline and aegirine crystals have grain size varying from 1 to 3 cm. Subhedral to euhedral arfvedsonite crystals occur with aegirine and K-feldspar and some of them have been altered to biotite. Fine-grained albite crystals occur along the margin of coarse-grained K-feldspar crystals, or within the large K-feldspar crystals (Fig. 5a and b). The major Nb–Ta-bearing mineral, pyrochlore, is closely associated with albite crystals in the margin of K-feldspar crystals (Fig. 5a, b and c), and is also associated with aegirine in some places (Fig. 5d). Pyrochlore crystals are euhedral in shape and brown in color, and they have grain sizes varying from 0.01 to 0.2 mm (Fig. 5d).

Accessory minerals include zircon, fergusonite, titanite, ilmenite, magnetite and fluorite. Euhedral to subhedral zircon grains vary in size from 0.1 to 0.5 mm and some grains show core–rim zonation. Euhedral or subhedral titanite grains range in size from 0.06 to 2.5 mm and some of them are altered and surrounded by albite.

3.2. Nb–Ta-poor syenitic dikes

Rocks of the Nb–Ta-poor syenitic dikes are composed of 60–80% K-feldspar, 5–10% plagioclase, ~5% albite, ~5% aegirine, ~5% arfvedsonite and ~2% biotite. The Nb–Ta-poor syenitic dikes contain much less albite than the Nb–Ta-mineralized dikes, consistent with weak albitization in the Nb–Ta-poor dikes. Fine-grained albite crystals make up a thin rim around K-feldspar (Fig. 5e). Pyrochlore is sporadically distributed in the Nb–Ta-poor dikes and is interstitial to K-feldspar and arfvedsonite. Epidote veinlet is observed in Nb–Ta-poor syenitic dikes (Fig. 5f). Accessory minerals include titanite, ilmenite, fergusonite, magnetite and fluorite, similar to those in the Nb–Ta-mineralized dikes.

3.3. Syenitic plutons

Rocks of the syenitic plutons are mainly composed of ~75% K-feldspar, 5–15% arfvedsonite, 1–5% aegirine and ~5% apatite with minor titanite, zircon, plagioclase, fluorite, biotite, ilmenite and magnetite. No albitization has been observed in the syenitic plutons.

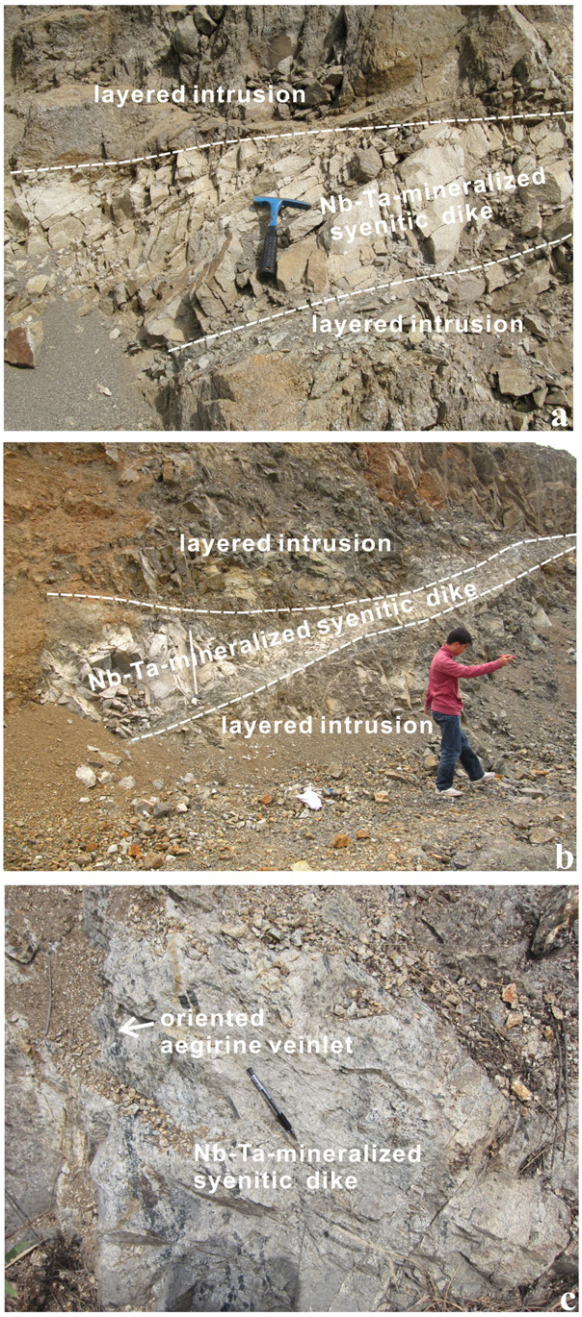

Fig. 4. Outcrop pictures showing a sharp boundary between the Nb–Ta-mineralized syenitic dikes and layered intrusion (a and b), and the aegirine veinlet is oriented along the long axis of the Nb–Ta-mineralized syenitic dikes (c).

4. Analytical methods

4.1. Whole-rock major and trace elements

Whole-rock major elements were analyzed by X-ray fluorescence on fused glass beads at the State Key Laboratory of Isotope Geochemistry, Guangzhou Institute of Geochemistry (GIG), Chinese Academy of Sciences (CAS). Rock samples were powdered to less than 200 mesh, and then fluxed with $Li_2B_4O_7$ (1:8) to make homogeneous glass disks at 1150–1200 °C using a V8C automatic fusion machine produced by the Anaymate Company in China.

Whole-rock trace elements, including REE, were determined with a Bruker M90 inductively coupled plasma mass spectrometry (ICP-MS) at the Guizhou TuoPu Resources and Environmental Analysis Center using the method of Qi et al. (2000). ~50 mg powdered sample was placed in a PTFE bomb and 1 ml of HF and 1 ml of HNO_3 were added. The sealed bombs were then placed in an electric oven and heated to 190 °C for about 36 h. After cooling, the bombs were heated on a hot plate to evaporate to dryness. 500 ng of Rh was added as an internal standard, and then 2 ml of HNO_3 and 4 ml of water were added. The bomb was again sealed and placed in an electric oven at 140 °C for about 5 h to dissolve the residue. After cooling, the final dilute factor is about 3000 for ICP-MS measurement. The sensitivity of the instrument was adjusted to about 500,000 cps (counts per second) for 1 ng ml^{-1} of ^{115}In and 200,000 cps for 1 ng ml^{-1} of ^{232}Th using the normal sensitivity mode. The accuracies of the ICP-MS analyses are estimated to be better than ±5 to 10% (relative) for most elements.

4.2. Mineral compositions

Mineral compositions were obtained with a JEOL JXA8100 electron microprobe at the State Key Laboratory of Isotope Geochemistry, GIGCAS, using an accelerating voltage of 15 kV, a beam current of 20 nA and a beam diameter of 1 μm. Both natural and synthetic standards were used: albite (Na), orthoclase (K), apatite (P), garnet (Mg, Si, Ca, Al), zircon (Zr, Hf), fluorite (F), monazite (Ce), metal Ta (Ta), metal Nb (Nb), metal U (U), rutile (Ti), yttrium (Y) and manganese oxide (Mn).

4.3. Whole-rock B concentration and B isotopic composition

Whole-rock B concentrations and B isotopic compositions were analyzed at the State Key Laboratory of Isotope Geochemistry, GIGCAS. About 150 mg of rock powder was precisely weighed and poured into a pre-cleaned 7 ml PFA beaker, then 100 ml mannitol, 100 ml H_2O_2 and 1 ml 24 M HF were added. The beaker was tightly capped and put on a hot plate at 60 °C for three days to extract B. Both the solution and deposit were then transferred into a pre-cleaned polypropylene (PP) tube, and centrifuged. The supernatant was collected, and most of B is concentrated in the solution, yielding a recovery of >99% (Wei et al., 2013). The collected supernatant was then diluted by Milli-Q water to make the HF concentration of 3 M for ion-exchange purification. The AG MP-1 strong anion exchange resin of the Bio-Rad company was selected for ion-exchange chromatographic purification. The eluted boron was collected in a pre-cleaned 15 ml PFA beaker, and quantitatively diluted to 12 ml.

A 2 ml aliquot of the elution was quantitatively taken for B measurement by using a Varian Vista Pro inductively coupled plasma atomic emission spectrometry (ICP-AES) equipped with a Teflon spray chamber and an Al_2O_3 injector, which was resistant to the corrosion of HF. Boron was detected at a wavelength of 249.678 nm. The measurement on the purified B is free from the influence of the large peak of Fe at 249.650 nm, and the detection limit is <10 ppb in the solution, which enables the analysis of samples with concentrations <1 ppm. The internal precision for B concentration is generally better than 5% (RSD). Two basalt standards with low B concentrations, B5 and BCR-2, were repeatedly measured along with the samples, yielding a B concentration of 9.1 ± 0.3 μg/g (1SD, n = 3) and 4.2 ± 0.3 μg/g (1SD, n = 3) for B5 and BCR-2, respectively. The accuracy of the results of B5 is better by 10% (RSD) compared to its certified value (~8.4 μg/g) (Tonarini et al., 2003).

The residual solution was used for $\delta^{11}B$ measurement. 100 ml of mannitol was added into the beaker to reduce volatilization loss of B during drying. The 15 ml PFA beaker was then put on a hot plate at 55 °C for two to three days. The dried samples were re-dissolved by 1.5 ml Milli-Q water. They were further diluted to ~100 ng ml^{-1} B. $\delta^{11}B$ analyses were performed using a Neptune MC-ICP-MS using

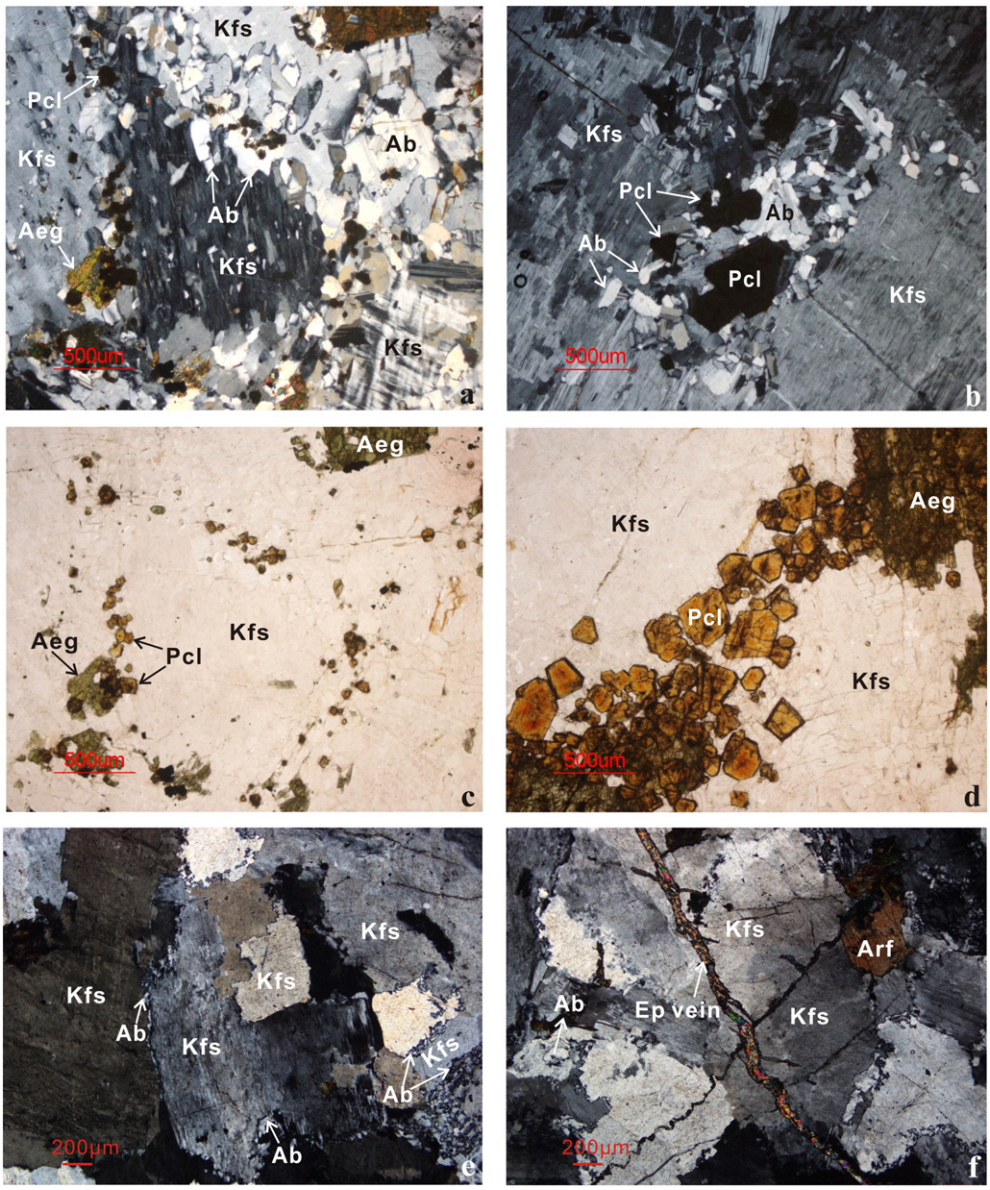

Fig. 5. Photomicrographs of rocks in the syenitic dikes. a—Fine-grained albite (Ab) crystals in the Nb–Ta-mineralized syenitic dike occur along the margin of coarse-grained K-feldspar (Kfs) crystals. Pyrochlore (Pcl) is closely associated with albite crystals. Under a cross-polarized and transmission light; b—fine-grained albite in the Nb–Ta-mineralized syenitic dike occurs within the large K-feldspar crystals. Pyrochlore (Pcl) is closely associated with albite crystals. Under a cross-polarized and transmission light; c—the same image of fig a showing that pyrochlore and albite crystals in the margin of K-feldspar crystals. Under a plane-polarized and transmission light; d—euhedral pyrochlore crystals in the Nb–Ta-mineralized syenitic dike are brown in color and present as aggregates with aegirine (Age). Under a plane-polarized and transmission light; e—very fine-grained albite crystals in the Nb–Ta-poor syenitic dike occur along the margin of coarse-grained K-feldspar (Kfs) crystals and form a narrow albite rim around the K-feldspar. Under a cross-polarized and transmission light; f—epidote (Ep) veinlet fills the cracks of the Nb–Ta-poor syenitic dike. Arf- arfvedsonite. Under a cross-polarized and transmission light.

sample-standard-bracketing (SSB) mode. Detailed analytical procedures of $\delta^{11}B$ are described by Wei et al. (2013). The internal precision for $\delta^{11}B$ was better than ±0.05% (2σ standard error), and the external precision for $\delta^{11}B$ was better than ±0.30% (2σ standard error) estimated by the long-term results of SRM 951 (Wei et al., 2013). Two basalt standards JB-2 and JB-3 were repeatedly analyzed along with the samples, yielding the $\delta^{11}B$ of 7.07‰ and 5.78‰. Boron isotopic compositions of the samples are presented as parts per mil deviations from NBS 951: $\delta^{11}B$ (‰) = $\{2 * (^{11}B/^{10}B)_{sample} / [((^{11}B/^{10}B)_{SRM951B} + (^{11}B/^{10}B)_{SRM951A}) - 1]\} \times 1000$ (Wei et al., 2013).

5. Analytical results

5.1. Whole-rock major and trace elements

Rocks of the Nb–Ta mineralized syenitic dikes have 62.0–66.9 wt.% SiO_2 and >10 wt.% $Na_2O + K_2O$ (Table 1 and Fig. 6), plotting in the syenite field in the TAS diagram (Fig. 7a). High $Na_2O + K_2O$ contents of the rocks are consistent with an alkaline affinity in the plot of total alkalis versus silica (Fig. 7b). They have A/CNK values ranging from 0.68 to 0.98, and are plotted in the peralkaline field in the plot of A/CNK versus

Table 1
Whole-rock major and trace element compositions of the Nb–Ta-mineralized syenitic dikes.

Locality	Luku mine											
Sample no.	LK-25	LK-27	LK-29	LK11-19	LK11-20	LK11-22	LK11-24	LK12-9	LK12-10	LK12-11	LK12-13	LK12-14
Major oxides (wt.%)												
SiO_2	65.8	64.7	64.1	65.3	64.9	66.0	64.8	64.1	64.7	63.5	65.7	63.4
TiO_2	0.42	0.73	1.91	0.18	0.22	0.10	1.10	0.56	0.32	0.20	0.56	0.66
Al_2O_3	17.7	15.8	16.6	16.7	16.1	17.6	17.7	16.0	16.2	14.6	17.4	14.9
Fe_2O_3	2.21	5.15	3.67	4.05	4.92	2.78	2.88	5.23	4.79	7.63	3.93	7.00
MnO	0.10	0.17	0.23	0.10	0.13	0.05	0.17	0.16	0.12	0.19	0.12	0.27
MgO	0.28	0.38	0.44	0.25	0.28	0.21	0.25	0.31	0.27	0.35	0.23	0.29
CaO	0.41	0.70	1.96	0.56	0.77	0.17	0.83	0.64	0.66	0.87	0.20	0.79
Na_2O	7.87	8.71	9.50	8.64	8.56	8.42	8.49	8.09	8.26	8.48	9.45	8.60
K_2O	4.58	3.05	1.01	3.70	3.62	3.94	3.27	3.97	4.07	3.56	1.92	3.62
P_2O_5	0.06	0.01	0.01	0.01	0.01	0.01	0.01	0.02	0.01	0.01	0.01	0.01
LOI	0.30	0.41	0.44	0.30	0.23	0.50	0.26	0.51	0.32	0.34	0.42	0.18
ANK	0.99	0.89	0.99	0.91	0.90	0.97	1.01	0.91	0.90	0.82	0.99	0.82
ACNK	0.95	0.83	0.82	0.87	0.83	0.95	0.93	0.85	0.84	0.75	0.97	0.76
K_2O+Na_2O	12.5	11.8	10.5	12.3	12.2	12.4	11.8	12.1	12.3	12.0	11.4	12.2
Trace elements (ppm)												
Ti	2520	4380	11,460	1080	1320	600	6600	3360	1920	1200	3360	3960
Sc	10.0	12.7	13.2	11.0	10.7	11.3	11.2	10.8	11.0	11.6	12.1	12.0
V	8.60	27.1	31.9	15.7	18.6	14.3	20.3	34.0	21.7	35.9	86.9	30.2
Cr	2.85	4.73	3.20	4.04	4.75	4.14	2.94	5.58	4.83	4.35	10.10	8.17
Co	5.20	4.59	15.8	6.13	4.65	3.95	3.77	2.04	1.37	2.08	3.57	2.27
Ni	5.77	15.6	10.3	6.84	6.55	9.74	2.08	5.34	3.76	3.80	5.77	6.32
Cu	6.14	8.37	12.1	5.76	4.82	4.20	14.8	12.6	6.20	4.57	12.8	8.10
Zn	168	133	542	77.8	83.5	65.7	129	126	109	158	152	181
Ga	51.9	71.2	74.9	61.3	54.9	70.9	51.6	62.2	55.8	46.9	55.9	49.9
Rb	175	114	22.5	152	142	210	115	198	184	158	73.4	213
Sr	138	102	185	65.2	66.8	37.0	382	119	88.8	38.6	46.5	66.6
Y	86.8	190	680	46.4	31.9	65.7	107	47.8	35.1	41.2	32.3	42.7
Zr	2350	8160	6620	798	923	935	2750	666	609	989	889	803
Nb	345	783	2210	215	280	213	371	229	394	206	393	1730
Cs	2.51	1.28	0.26	0.87	0.80	3.81	1.54	0.89	1.07	0.88	0.68	1.74
Ba	139	149	67.8	137	132	116	126	244	230	171	188	197
La	214	1200	1060	243	305	17.2	235	1230	887	48.0	18.2	101
Ce	373	1760	1420	388	454	34.7	415	1810	1250	75.2	38.9	207
Pr	39.7	178	125	36.5	44.1	3.84	41.3	169	115	8.09	4.46	23.0
Nd	127	539	388	115	138	13.4	136	491	333	26.8	16.4	71.2
Sm	20.7	68.8	84.2	14.7	16.2	3.68	21.2	53.4	36.5	5.14	3.68	13.5
Eu	2.82	7.16	10.37	1.42	1.70	0.58	2.50	4.63	3.36	0.73	0.56	1.70
Gd	17.5	30.8	71.2	9.19	9.18	3.50	12.4	20.8	13.2	4.01	2.91	7.34
Tb	2.87	8.05	16.99	1.92	1.89	1.01	3.19	5.02	3.43	0.96	0.73	1.85
Dy	14.3	35.7	101	8.64	7.20	7.50	17.0	12.5	9.52	5.97	4.67	9.08
Ho	2.96	7.51	20.5	1.69	1.35	1.81	3.62	2.00	1.54	1.32	1.05	1.64
Er	9.48	26.7	59.4	5.65	4.65	6.21	11.8	8.00	5.75	4.86	3.47	4.86
Tm	1.43	3.95	8.27	0.83	0.68	1.10	1.79	0.84	0.65	0.95	0.59	0.73
Yb	9.56	28.2	48.1	6.04	5.64	7.12	11.6	7.28	5.50	8.88	4.58	6.09
Lu	1.35	4.13	5.90	0.99	1.01	0.98	1.68	1.26	0.98	1.61	0.76	1.13
Hf	45.9	155	129	25.3	28.8	29.6	62.6	26.5	21.9	46.8	29.3	33.6
Ta	25.3	62.2	64.0	13.1	21.0	10.8	14.6	12.0	26.8	17.5	20.8	149
Th	62.4	191	1760	41.1	33.4	42.9	85.8	78.9	68.4	25.9	24.4	63.3
U	52.1	140	66.6	12.8	24.6	4.07	11.1	9.10	47.9	23.4	11.2	243
REE	923	4088	4099	880	1022	168	1021	3864	2701	234	133	493
Eu/Eu*	0.44	0.41	0.40	0.35	0.39	0.49	0.43	0.36	0.38	0.47	0.51	0.47

Locality	Baicao mine											
Sample no.	BC-3	BC-5	BC-8	BC-10	BC-13	BC-14	BC-19	BC11-1	BC11-2	BC11-7	BC11-8	BC11-25
Major oxides (wt.%)												
SiO_2	63.9	63.8	62.7	63.2	64.3	64.1	62.0	64.9	63.5	66.9	64.7	62.7
TiO_2	0.81	0.67	0.88	1.73	0.86	0.82	1.74	0.40	0.49	0.41	0.30	0.28
Al_2O_3	18.0	15.8	14.5	16.4	14.7	15.5	16.3	17.1	15.2	14.7	15.8	17.9
Fe_2O_3	2.74	5.05	5.40	4.85	5.73	5.16	4.36	2.94	5.01	4.75	6.08	5.39
MnO	0.11	0.25	0.17	0.25	0.28	0.21	0.19	0.11	0.29	0.19	0.27	0.03
MgO	0.64	0.54	2.08	0.60	0.58	0.60	1.47	0.45	1.64	0.26	0.39	0.26
CaO	1.38	0.77	3.24	1.33	0.87	0.90	2.31	0.53	2.74	0.65	0.76	0.82
Na_2O	8.15	7.44	7.44	7.90	6.76	6.72	7.89	6.45	7.26	6.77	8.61	6.70
K_2O	3.42	4.87	2.98	2.79	5.02	5.17	2.65	6.19	3.13	4.73	2.80	5.24
P_2O_5	0.12	0.11	0.04	0.24	0.08	0.09	0.39	0.02	0.10	0.03	0.01	0.00
LOI	0.39	0.16	0.20	0.38	0.28	0.23	0.31	0.41	0.31	0.18	0.10	0.16
ANK	1.05	0.90	0.94	1.02	0.89	0.93	1.03	0.99	0.99	0.91	0.92	1.07
ACNK	0.92	0.83	0.68	0.89	0.81	0.85	0.81	0.94	0.75	0.84	0.85	0.98
K_2O+Na_2O	11.6	12.3	10.4	10.7	11.8	11.9	10.5	12.6	10.4	11.5	11.4	11.9

Table 1 *(continued)*

Locality	Luku mine											
Sample no.	LK-25	LK-27	LK-29	LK11-19	LK11-20	LK11-22	LK11-24	LK12-9	LK12-10	LK12-11	LK12-13	LK12-14
Trace elements (ppm)												
Ti	4860	4020	5280	10,380	5160	4920	10,440	2400	2940	2460	1800	1680
Sc	10.2	10.2	17.4	9.6	10.6	10.2	10.3	8.6	13.4	10.4	11.4	11.9
V	32.1	6.02	89.6	45.8	3.99	3.98	44.9	5.80	38.9	6.00	10.1	19.5
Cr	2.74	2.57	105	3.99	3.71	2.62	3.06	3.35	3.38	2.95	3.20	2.82
Co	4.73	1.70	10.7	5.77	0.71	0.85	6.74	1.08	6.61	1.01	1.44	3.00
Ni	8.58	2.37	48.8	5.61	1.95	1.84	3.79	1.63	4.60	1.99	2.70	3.85
Cu	31.3	7.25	27.2	57.4	6.96	8.08	24.8	7.30	8.95	4.97	3.87	10.5
Zn	121	188	194	261	305	186	131	123	261	168	379	85.4
Ga	30.4	43.0	62.0	49.8	36.6	30.7	30.9	37.3	37.2	47.2	55.5	50.7
Rb	145	298	222	127	264	203	135	296	174	297	173	273
Sr	1290	73.4	239	957	43.2	43.5	1170	94.2	561	75.5	48.2	249
Y	84.1	49.7	105	172	113	71.4	135	79.5	205	132	132	166
Zr	2500	433	3340	4160	1010	1000	2200	1580	3050	3040	923	3450
Nb	224	244	169	393	336	158	322	231	336	392	800	539
Cs	1.71	0.51	3.74	1.80	1.04	1.60	2.12	0.55	1.19	0.42	0.93	1.14
Ba	1780	262	274	1030	475	563	1260	298	372	247	35.0	269
La	77.5	110	138	322	226	132	137	153	132	585	70.5	400
Ce	155	251	242	525	470	257	280	289	249	1060	149	605
Pr	20.2	33.4	26.3	55.6	57.1	31.6	35.0	31.5	31.0	118	18.0	56.2
Nd	79.5	125	95.1	193	215	112	136	111	114	401	67.4	171
Sm	20.1	25.7	18.4	33.5	42.0	21.0	32.0	19.5	27.3	64.2	16.4	26.6
Eu	3.40	3.71	2.27	4.58	5.27	3.17	4.72	2.43	4.92	6.12	1.53	2.26
Gd	16.1	16.0	13.2	26.4	25.5	14.9	24.1	13.4	25.3	36.4	13.6	18.5
Tb	3.44	3.27	3.07	5.58	5.74	2.98	5.34	2.87	5.48	7.71	3.27	4.54
Dy	19.0	14.1	17.0	30.2	27.4	14.7	29.1	14.3	33.0	33.5	20.5	25.7
Ho	3.45	2.25	3.43	6.28	4.77	2.73	5.32	2.75	6.93	6.22	4.22	5.62
Er	9.48	5.82	10.5	19.6	12.5	7.87	14.7	7.77	20.8	19.1	13.2	18.3
Tm	1.24	0.66	1.65	2.83	1.46	0.99	1.91	1.04	3.01	2.42	2.15	2.85
Yb	7.80	4.46	11.6	18.8	8.41	6.43	11.56	6.50	19.0	15.4	14.9	18.5
Lu	0.97	0.71	1.71	2.53	1.18	0.90	1.46	0.92	2.63	2.25	2.13	2.51
Hf	68.1	12.6	86.6	99.5	20.1	21.9	60.2	34.4	72.6	56.8	37.0	73.3
Ta	17.1	17.6	10.3	24.0	22.8	10.6	25.7	11.8	17.0	24.6	54.4	35.9
Th	41.1	39.7	96.7	104	24.3	20.7	54.6	56.0	103	78.8	81.7	114
U	12.0	13.6	10.6	26.5	14.2	5.72	10.6	12.3	12.0	27.4	31.9	28.0
REE	501	646	689	1418	1215	680	853	735	879	2489	529	1524
Eu/Eu*	0.56	0.52	0.43	0.45	0.46	0.52	0.50	0.44	0.56	0.35	0.30	0.30

A/NK (Fig. 7c). The rocks have 133 to 4088 ppm REE and have LREE-enriched patterns with negative Eu anomalies (Eu/Eu* = 0.30–0.56) on the chondrite-normalized REE diagrams (Fig. 8a). They contain 158–2210 ppm Nb, 10.3–149 ppm Ta and 433–8160 ppm Zr (Table 1), and have positive Rb, Th, Nb, Ta and Zr anomalies and negative Ba, Sr and Ti anomalies on the primitive mantle-normalized trace element patterns (Fig. 8b).

Rocks of the Nb–Ta-poor syenitic dikes have 60.1–63.4 wt.% SiO_2, slightly lower than those of the Nb–Ta-mineralized dikes. They have total alkalis ($Na_2O + K_2O$) of 9.68–11.4 wt.% (Table 2) and are also plotted in the field of syenite (Fig. 7a). The A/CNK ratios of the rocks vary from 0.75 to 0.98, which are between the metaluminous and peralkaline fields in the plot of A/CNK versus A/NK (Fig. 7c). They contain 117–394 ppm REE and have slightly LREE-enriched patterns with positive Eu anomalies (Eu/Eu* = 0.72–1.87) (Fig. 8c). They have 34.2–125 ppm Nb and 1.31–8.93 ppm Ta, much lower than those of the Nb–Ta-mineralized syenitic dikes (Fig. 9a and b). Likewise, the samples of the Nb–Ta-poor syenitic dikes contain 125–544 ppm Zr, much lower than those of the Nb–Ta-mineralized syenitic dikes. They have relatively flat trace element patterns with weakly positive Ba and Sr anomalies and negative Ti anomalies (Fig. 8d).

Rocks of the syenitic plutons have 62.4–65.5 wt.% SiO_2 and 11.5–12.8 wt.% $Na_2O + K_2O$ (Table 3). They are of peralkaline in the plot of A/CNK versus A/NK (Fig. 7c). Most samples have REE and trace element concentrations similar to those of the Nb–Ta-poor syenitic dikes and have negative Eu anomalies on the REE patterns with Eu/Eu* of 0.55–0.91, and negative Sr and Ti anomalies and positive Ba anomalies on the trace element patterns (Fig. 8e and f).

5.2. Mineral chemistry

Pyrochlore is the major Nb- and Ta-bearing mineral in the syenitic dikes. The chemical formula of pyrochlore is $(Ca,Na)_2Nb_2O_6(OH,F)$ and theoretically it contains 15.41 wt.% CaO, 8.25 wt.% Na_2O, 73.05 wt.% Nb_2O_5 and 5.22 wt.% F. The pyrochlore crystals in the Nb–Ta-mineralized syenitic dikes have 11.4–17.4 wt.% CaO, 0.81–5.06 wt.% Na_2O, 46.8–51.3 wt.% Nb_2O_5 and 1.62–3.45 wt.% F (Table 4), much less than the theoretical values. Instead they contain 2.88–7.01 wt.% Ce_2O_3, 4.83–7.67 wt.% UO_2, 8.26–10.2 wt.% TiO_2, 0.68–4.84 wt.% ThO_2 and 2.62–3.62 wt.% Ta_2O_5 (Table 4), indicating that Ce, U, Ti, Th and Ta may substitute for Nb in the lattice of the pyrochlore crystal. However, the total amounts of the oxides in the pyrochlore grains are less than 100 wt.% due to the presence of volatile (Table 4). The pyrochlore crystals in the Nb–Ta-poor syenitic dikes have 15.7–17.1 wt.% CaO, higher than that of the grains in the Nb–Ta-mineralized syenitic dikes. On the other hand, they have 2.44–3.74 wt.% Na_2O, 44.0–47.4 wt.% Nb_2O_5 and 1.91–2.24 wt.% F (Table 4), much lower than those of the grains in the Nb–Ta-mineralized syenitic dikes.

Accessory mineral titanite in the syenitic dikes also contains minor Nb, Ce and Yb (Table 5). The chemical formula of titanite is $CaTiSiO_5$ and theoretically it contains 28.6 wt.% CaO, 40.8 wt.% TiO_2 and 30.6 wt.% SiO_2. The titanite crystals in the Nb–Ta-mineralized syenitic

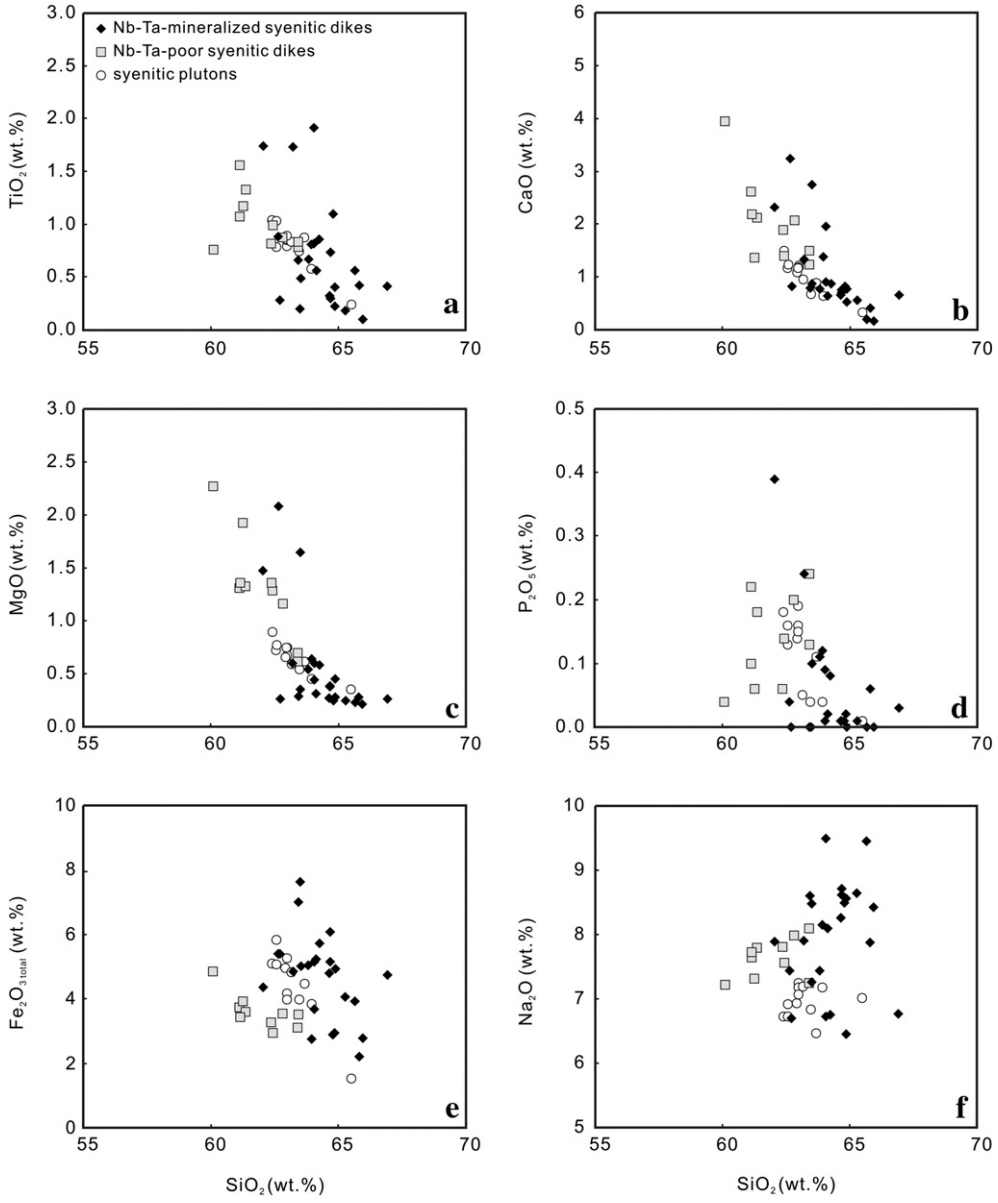

Fig. 6. Plots of SiO_2 versus CaO (a), P_2O_5 (b), TiO_2 (c), MgO (d), Fe_2O_{3total} (e) and Na_2O (f) for the rocks of the Nb–Ta-mineralized and Nb–Ta-poor syenitic dikes and syenitic plutons.

dikes have 20.0–28.9 wt.% CaO, 36.1–38.1 wt.% TiO_2 and 28.6–29.5 wt.% SiO_2, slightly lower than the theoretical values. However, they contain 1.78–3.86 wt.% Nb_2O_5, 1.43–2.55 wt.% Ce_2O_3 and 0.41–0.89 wt.% Y_2O_5 (Table 5). A few titanite crystals in the dikes have zonation in composition; the rim that is surrounded by albite has Na_2O, Ce_2O_3 and Nb_2O_5 higher than the core. The titanite crystals in the Nb–Ta-poor syenitic dikes have 25.5–28.9 wt.% CaO, 34.3–37.0 wt.% TiO_2 and 29.3–29.8 wt.% SiO_2. They contain 0.41–2.82 wt.% Nb_2O_5, 0.41–1.70 wt.% Ce_2O_3 and 0.02–0.18 wt.% Y_2O_5, lower than those of the grains in the Nb–Ta-mineralized syenitic dikes.

5.3. Whole-rock B concentrations and B isotopic compositions

Rocks of the Nb–Ta-mineralized syenitic dikes have 11.4–23.9 ppm B and $\delta^{11}B$ values ranging from −17.95 to −14.54‰ (Table 6). Rocks of the Nb–Ta-poor syenitic dikes and syenitic plutons have B concentrations varying from 3.32 to 16.5 ppm, and $\delta^{11}B$ values from −13.45 to −10.02‰ (Table 6). The samples of the Nb–Ta-mineralized syenitic dikes have B concentrations higher and $\delta^{11}B$ values lower than those of the Nb–Ta-poor dikes (Fig. 10a).

6. Discussion

6.1. Fractionation of K-feldspar and plagioclase

Rocks of the Nb–Ta-mineralized and Nb–Ta-poor syenitic dikes and the syenitic pluton have similar mineral assemblages but with different mineral modes. Rocks of the Nb–Ta-mineralized syenitic dikes have less K-feldspar than the rocks of the Nb–Ta-poor syenitic dikes and syenitic pluton. There are linear trends of TiO_2, CaO, MgO and P_2O_5 against SiO_2 for the Nb–Ta-mineralized and Nb–Ta-poor syenitic dikes (Fig. 6a, b, c and d), consistent with the fractionation of Ti-bearing phases (such as ilmenite and titanite), plagioclase, mafic mineral (arfvedsonite and biotite) and apatite. The variation of Fe_2O_{3total} (Fig. 6e) is consistent with variable modes of aegirine in the Nb–Ta-mineralized and Nb–Ta-poor syenitic dikes.

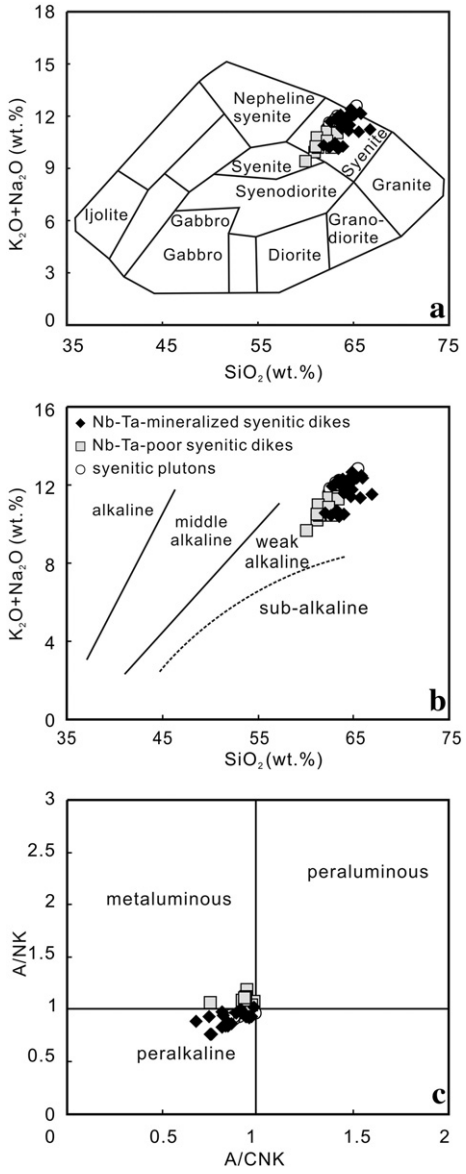

Fig. 7. TAS diagram (a), total alkalis versus SiO_2 (b) and molecular A/NK [Al_2O_3 / (Na_2O + K_2O)] versus A/NCK [Al_2O_3 / (Na_2O + CaO + K_2O)] (c) for the rocks of the Nb–Ta-mineralized and Nb–Ta-poor syenitic dikes and syenitic plutons.

The Nb–Ta-mineralized syenitic dikes have negative Eu anomalies (Fig. 8a), whereas the Nb–Ta-poor syenitic dikes have positive Eu anomalies on the REE patterns (Fig. 8c). The variation of Eu anomalies is mainly related to the extent of fractionation of plagioclase (Drake and Weill, 1975; Weill and Drake, 1973). The positive Eu anomalies of the Nb–Ta-poor syenitic dikes are comparable with the metaluminous syenitic plutons in the Panxi region (Shellnutt and Zhou, 2007; Shellnutt et al., 2008; Zhong et al., 2009). The metaluminous syenitic plutons are considered to have formed from remelting of plagioclase-rich mafic cumulates (Shellnutt and Zhou, 2007), Therefore, we consider that the Nb–Ta-mineralized and Nb–Ta-poor syenitic dikes may have originated from remelting of mafic cumulates that are rich in plagioclase, however, the Nb–Ta-mineralized syenitic dikes may have experienced more intensive fractionation of plagioclase than the Nb–Ta-poor dikes so that they have negative Eu anomalies on the REE patterns. This is consistent with the variations of Ba, Rb and Sr concentrations of the rocks. Rocks of the Nb–Ta-mineralized syenitic dikes have highly variable Sr and Ba concentrations and a weakly positive correlation of Sr and Ba, consistent with the fractionation of K-feldspar and plagioclase (Fig. 11a). In contrast, rocks of the Nb–Ta-poor syenitic dikes and syenitic plutons have highly variable Sr against restricted Ba concentrations, consistent with the fractionation of plagioclase (Fig. 11a).

6.2. Nb–Ta-mineralized syenitic dikes from highly evolved magma

Boron is highly incompatible and has low partition coefficient ($D_B^{mineral/melt}$) in olivine, pyroxene, amphibole and feldspar (Brenan et al., 1998; Klemme et al., 2002). The rocks of the Nb–Ta-poor syenitic dikes have 3.32 to 16.5 ppm B, much lower than those of the Nb–Ta-mineralized syenitic dikes (11.3 to 23.8 ppm) (Table 6 and Fig. 10a), indicating that the Nb–Ta-mineralized syenitic dikes may have formed from more evolved magma.

Rubidium has ionic radius larger than K, the energy of the K – O bond is stronger than the Rb – O bond. Therefore, Rb is mildly compatible with K-feldspar, whereas K is highly compatible with K-feldspar. The K/Rb of residual magmas thus decreases with the fractionation of K-feldspar (Dostal and Chatterjee, 2000). Strontium prefers to concentrate in the early crystallized phases, resulting in the increase of Rb/Sr of the magma with fractionation process (Yang et al., 2009). Rocks of the Nb–Ta-mineralized syenitic dikes have K/Rb of 111 to 236, lower than that of the Nb–Ta-poor syenitic dikes (200 to 450). On the other hand, they have Rb/Sr of 1.1 to 6.1, much higher than that of the Nb–Ta-poor syenitic dikes (<1) (Fig. 11b), indicating that the Nb–Ta-mineralized syenitic dikes may have formed from highly evolved magma.

Pyrochlore crystals in the Nb–Ta-mineralized syenitic dikes contain 1.62–3.45% F, indicating that the magma of the Nb–Ta-mineralized syenitic dikes may be rich in volatile/fluid. This is similar to the Yichun Li–F granitic pluton which hosts No. 414 Nb–Ta deposit in South China (Yin et al., 1995). The high volatile and fluid contents of the magmas also support that the magma of the Nb–Ta-mineralized syenitic dikes formed from highly evolved magma. The highly evolved magma may have low viscosity at the presence of large amounts of volatile and fluid, the aligned aegirine veinlet in the Nb–Ta-mineralized syenitic dikes (Fig. 4c) can thus be explained as that the aegirine crystals were removed and orientated with the emplacement of the Nb–Ta-mineralized syenitic dikes.

6.3. A transition from magmatic to hydrothermal stage

The variation of $\delta^{11}B$ of the rocks could be attributed to different magma sources, fractionation of magma, crustal contamination and magma-derived fluids (Kaliwoda et al., 2011). Rocks of the Nb–Ta-mineralized and Nb–Ta-poor syenitic dikes have similar ε_{Nd} values (−0.2 to +0.2 for the Nb–Ta-mineralized dikes and −0.8 to +0.7 for the Nb–Ta-poor syenitic dikes) (our unpublished data), indicating that they may have formed from a similar source, ruling out the possibility that they may have been derived from different source magmas.

Unless sodalite crystallizes from magmas, which would significantly decrease the $\delta^{11}B$ value of the residual magmas, the fractionation process is believed to insignificantly affect the variation of $\delta^{11}B$ values of magmas at temperatures ranging from 450 to 750 °C because of the low partition coefficient of B to the minerals such as amphibole, feldspar and pyroxene (Kaliwoda et al., 2011). Note that the rocks of the Nb–Ta-mineralized syenitic dikes have $\delta^{11}B$ values ranging from −17.95 to −14.54‰, only slightly lower than those of the Nb–Ta-poor syenitic dikes and syenitic pluton (−13.45 to −10.02‰). It is thus unlikely that there was a substantial fractionation of sodalite during the formation of the Nb–Ta-mineralized and Nb–Ta-poor syenitic dikes.

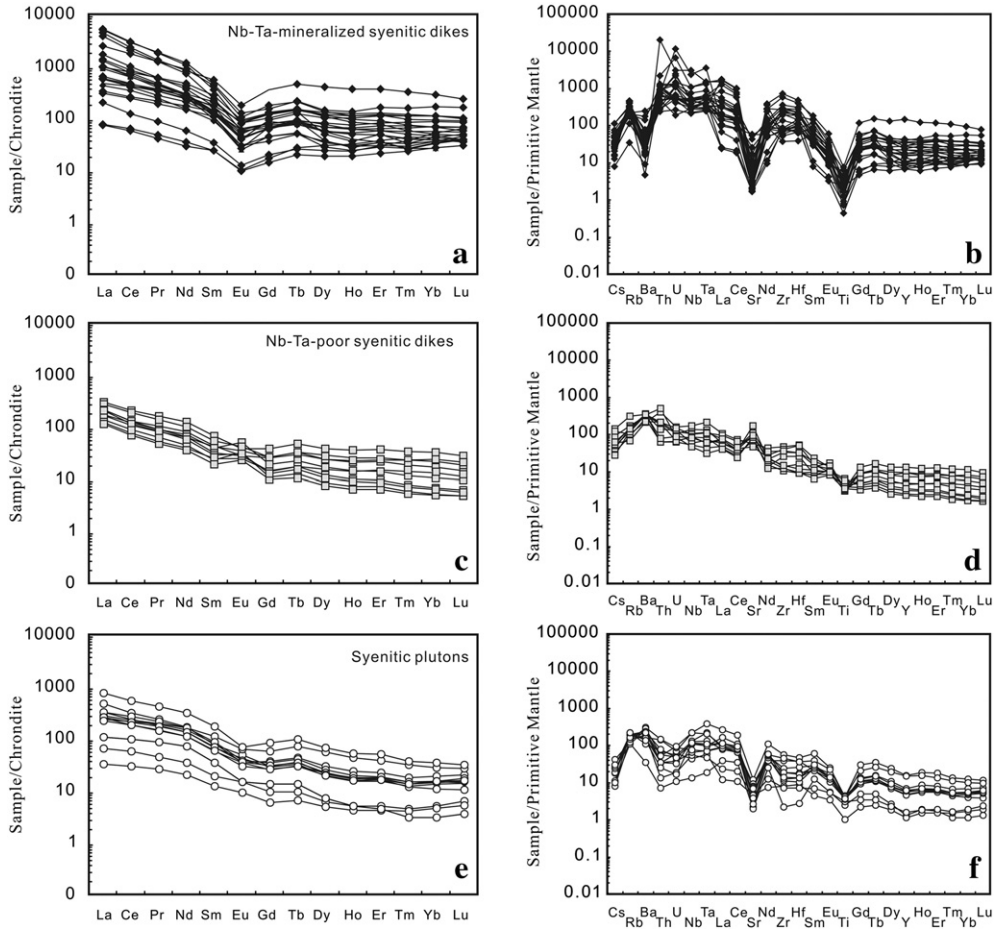

Fig. 8. Chondrite-normalized rare earth element patterns and primitive mantle-normalized trace element patterns for the rocks of the Nb–Ta-mineralized and Nb–Ta-poor syenitic dikes and syenitic plutons.
Normalizing values are from Sun and McDonough (1989a, 1989b).

The Nb–Ta-mineralized and Nb–Ta-poor syenitic dikes and syenitic plutons in the Panxi region have $\delta^{11}B$ values similar to those of terrestrial sediments, far below the value of seawater and/or fluid (Garda et al., 2009) (Fig. 10b). The relatively low $\delta^{11}B$ values of the Nb–Ta-mineralized syenitic dikes may be caused by rock–fluid reaction. In theory, both B concentrations and $\delta^{11}B$ values of rocks would decrease when the rocks experienced external fluid alteration, because B would be leached by fluids. However, the Nb–Ta-mineralized syenitic dikes have $\delta^{11}B$ values slightly lower than the Nb–Ta-poor syenitic dikes but have B concentrations much higher than the Nb–Ta-poor syenitic dikes and syenitic plutons. Therefore, it is unlikely that the low $\delta^{11}B$ values of the Nb–Ta-mineralized syenitic dikes are resulted from external fluid alteration.

A possible explanation for the low, negative $\delta^{11}B$ values of the Nb–Ta-mineralized syenitic dikes is that the fluids exsolved from the highly evolved magmas in the late stage. It is believed that the compound with the higher isotope fractionation factor ratio (/ ′) preferentially incorporates heavier isotope (Oi et al., 1989). The / ′ of the threefold coordinated $B(OH)_3$ site is higher than the fourfold coordinated $B(OH)_4^-$ site at the same temperature and pressure. Therefore the $B(OH)_3$ site preferentially incorporates ^{11}B, whereas the $B(OH)_4^-$ site prefers ^{10}B (Kakihana et al., 1977, 1982). The $\delta^{11}B$ values of the rocks are thus dependent on the ratio of $B(OH)_3$ and $B(OH)_4^-$, which, in turn, is mainly controlled by the pH values of fluids. At pH > 9, B is predominantly tetrahedrally coordinated in $B(OH)^{4-}$ groups, resulting in a decrease of $\delta^{11}B$ values of the rocks. In neutral and acidic (pH ≤ 7) hydrous fluids, it is trigonally coordinated in $B(OH)_3$ units, resulting in an increase of $\delta^{11}B$ values of the rocks (Hershry et al., 1986; Kakihana et al., 1977). However, the pH values of the fluids of highly evolved alkaline magmas are estimated to be between 8 and 10 (Markl and Baumgartner, 2002). In this range, the ratio of $B(OH)_3$ and $B(OH)_4^-$ has a poor correlation with pH values, therefore, the variation of $\delta^{11}B$ values of rocks is not only controlled by the pH values of fluids.

It is considered that B usually enters the $B(OH)_4^-$ site in melts, whereas it occurs as $B(OH)_3$ in hydrous fluids (Kakihana et al., 1977, 1982; Oi et al., 1989; Palmer and Swihart, 1996). Silicate minerals amphibole, mica, pyroxene and feldspar prefer to incorporate B as $B(OH)_4^-$ substituting for Si, and would therefore fractionate ^{10}B of melts so that the rocks formed from less evolved magmas would have high $\delta^{11}B$ values (Hervig et al., 2002; Tonarini et al., 2003; Werding and Schreyer, 2002). On the other hand, when magmas evolved to a solid–melt-fluid stage, ^{11}B prefers fluids that exsolved from highly evolved magma in the late stage so that the rocks formed from the highly evolved magma would have low $\delta^{11}B$ values. Therefore, the relatively low $\delta^{11}B$ values of the Nb–Ta-mineralized syenitic dikes indicate a highly evolved, fluid-rich magma in a transitional, magmatic–hydrothermal stage of magma evolution. The pegmatitic

Table 2
Whole-rock major and trace element compositions of the Nb–Ta-poor syenitic dikes.

Locality	Luku mine		Baicao mine							
Sample no.	LK-12	LK-16	BC-4	BC11-6	BC11-11	BC11-15	BC11-17	BC11-18	BC11-19	BC11-20
Major oxides (wt.%)										
SiO_2	62.4	61.3	61.1	62.8	60.1	63.4	63.4	62.4	61.4	61.1
TiO_2	0.99	1.17	1.07	0.87	0.76	0.78	0.83	0.82	1.33	1.56
Al_2O_3	18.4	18.2	19.0	18.0	16.3	17.8	18.4	18.4	18.4	18.4
Fe_2O_3	2.95	3.92	3.72	3.54	4.84	3.52	3.11	3.28	3.61	3.42
MnO	0.06	0.09	0.09	0.10	0.10	0.09	0.08	0.06	0.09	0.08
MgO	1.28	1.92	1.31	1.16	2.27	0.70	0.62	1.36	1.32	1.36
CaO	1.40	1.37	2.61	2.07	3.95	1.49	1.24	1.89	2.12	2.18
Na_2O	7.56	7.31	7.65	7.99	7.22	7.24	8.09	7.81	7.80	7.73
K_2O	3.79	3.70	2.53	2.44	2.46	4.14	3.19	3.04	2.65	2.78
P_2O_5	0.14	0.06	0.10	0.20	0.04	0.13	0.24	0.06	0.18	0.22
LOI	0.48	0.44	0.38	0.51	1.35	0.17	0.44	0.55	0.72	0.65
ANK	1.11	1.13	1.24	1.14	1.12	1.09	1.10	1.14	1.17	1.17
ACNK	0.96	0.98	0.95	0.92	0.75	0.93	0.97	0.94	0.94	0.93
K_2O+Na_2O	11.4	11.0	10.2	10.4	9.68	11.4	11.3	10.9	10.5	10.5
Trace elements (ppm)										
Ti	5940	7020	6420	5220	4560	4680	4980	4920	7980	9360
Sc	8.97	8.21	10.2	9.80	10.7	9.44	10.4	11.0	10.2	9.61
V	38.8	42.4	64.9	41.7	67.8	30.7	42.9	53.8	52.2	47.8
Cr	2.35	2.65	3.98	4.21	3.88	2.97	3.44	6.84	4.12	10.8
Co	5.91	8.32	7.43	5.48	10.30	2.96	3.76	6.24	7.40	7.72
Ni	2.98	2.34	8.86	5.98	17.6	3.21	3.21	5.59	5.89	9.51
Cu	18.5	10.6	28.4	10.7	17.0	8.7	12.1	15.7	22.1	19.2
Zn	57.7	110.4	91.7	65.4	98.8	82.8	95.2	63.5	78.3	72.7
Ga	23.1	23.1	24.4	24.3	21.3	23.4	23.9	23.3	24.8	23.4
Rb	60.5	199	110	44.4	67.8	79.3	97.2	77.1	92.8	101
Sr	1470	1670	3740	1210	2380	1020	1600	1820	2030	2070
Y	12.4	24.3	44.9	62.0	45.1	22.4	35.2	11.4	17.2	15.6
Zr	125	296	386	544	469	159	418	146	173	145
Nb	38.0	62.0	101.0	125.0	76.4	43.3	74.8	34.2	59.4	64.6
Cs	1.10	4.66	2.96	1.95	4.04	0.91	1.36	1.68	2.11	1.81
Ba	1920	2460	2230	1510	1580	2550	2510	2390	2500	2510
La	33.9	29.7	40.8	74.2	52.9	41.6	67.4	28.4	52.9	50.0
Ce	55.9	48.7	68.4	132.0	83.2	77.0	120	43.5	81.4	71.7
Pr	6.20	5.24	8.02	15.9	10.3	8.83	13.4	4.67	8.86	8.28
Nd	22.0	19.5	30.5	60.6	38.9	34.2	48.9	17.3	31.6	27.6
Sm	3.73	3.94	6.78	10.7	7.01	6.36	8.64	3.05	5.10	4.60
Eu	1.96	1.49	2.11	2.29	1.72	3.05	2.53	1.41	1.70	1.84
Gd	2.39	3.15	5.73	8.12	5.42	4.14	5.63	2.13	3.08	2.73
Tb	0.50	0.69	1.27	1.83	1.16	0.89	1.26	0.42	0.69	0.60
Dy	2.32	4.08	7.58	10.10	6.41	4.48	6.33	2.03	3.19	2.81
Ho	0.44	0.84	1.50	2.10	1.34	0.85	1.26	0.39	0.59	0.54
Er	1.27	2.57	4.42	6.35	4.08	2.44	3.78	1.13	1.70	1.51
Tm	0.16	0.37	0.62	0.90	0.62	0.31	0.50	0.15	0.21	0.19
Yb	0.94	2.37	3.83	5.77	4.22	1.88	3.05	0.90	1.25	1.17
Lu	0.13	0.30	0.49	0.74	0.57	0.26	0.39	0.13	0.17	0.15
Hf	2.92	8.26	10.3	16.6	16.2	5.13	10.5	3.11	3.81	2.96
Ta	1.83	3.40	5.61	8.93	4.85	3.00	4.55	1.31	2.58	2.47
Th	5.47	17.3	17.5	35.0	18.4	11.9	18.9	42.9	6.90	5.50
U	1.36	1.45	2.30	3.48	2.52	2.85	3.19	1.84	1.87	1.39
REE	144	147	227	394	263	209	318	117	210	189
Eu/Eu*	1.87	1.26	1.01	0.72	0.82	1.71	1.04	1.61	1.22	1.46

texture of the Nb–Ta-mineralized syenitic dikes is consistent with that they formed in a fluid-rich, magmatic–hydrothermal stage (c.f. Bakker and Elburg, 2006).

6.4. Albitization and enrichment of Nb and Ta

The linear trends of Nb and Ta against SiO_2 for the Nb–Ta-mineralized and Nb–Ta-poor syenitic dikes (Fig. 9a and b) indicate that Nb and Ta tend to be enriched in more evolved magma. The pyrochlore crystals in the Nb–Ta-mineralized syenitic dikes have Nb_2O_5 and F contents higher than those in the Nb–Ta-poor syenitic dikes (Fig. 12b). The rim of a pyrochlore crystal has higher Nb and F than the core part (Table 4), indicating that Nb and F tend to be enriched in the late stage of the highly evolved magma.

The rocks of the Nb–Ta mineralized syenitic dikes have higher Na_2O and lower CaO contents than those of the Nb–Ta-poor syenitic dikes (Fig. 6f). Likewise, the pyrochlore crystals in the Nb–Ta-mineralized syenitic dikes have higher Na_2O and lower CaO contents than those in the Nb–Ta-poor syenitic dikes (Fig. 12a). There are positive correlations of Na_2O, Nb, and Ta for the rocks of the Nb–Ta-mineralized and Nb–Ta-poor syenitic dikes (Fig. 9c and d), indicating that the enrichment of Nb and Ta in the Nb–Ta-mineralized syenitic dikes is likely related to the increase of Na. Given that the large amounts of fine-grained albite crystals in the Nb–Ta-mineralized syenitic dikes formed due to albitization, the enrichment of Nb and

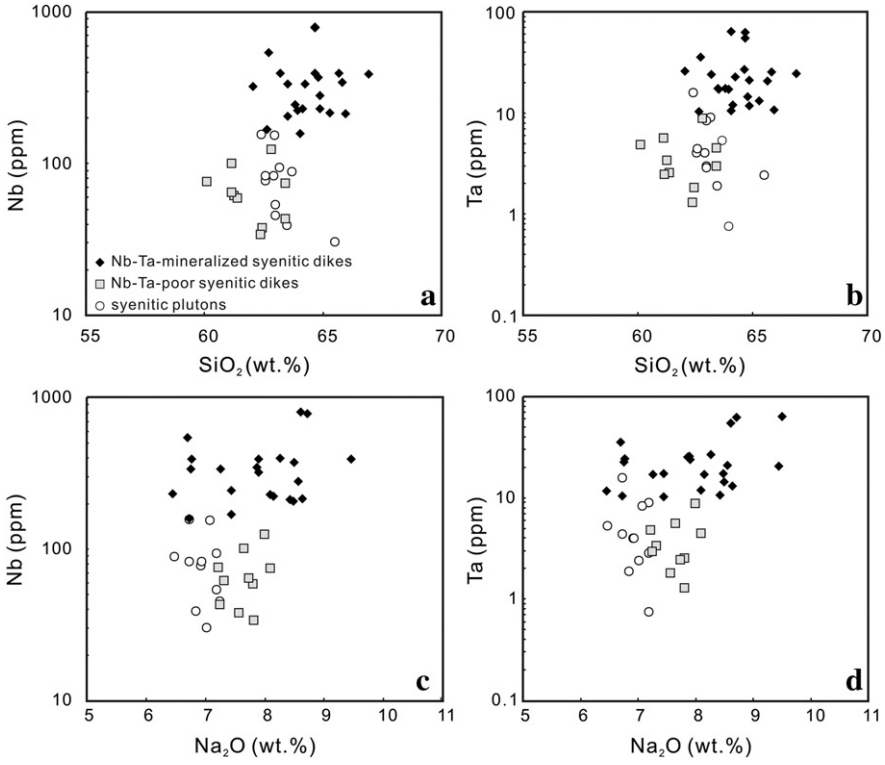

Fig. 9. Plots of SiO_2 versus Nb and Ta (a and b), Na_2O versus Nb and Ta (c and d) for the rocks of the Nb–Ta-mineralized and Nb–Ta-poor syenitic dikes and syenitic plutons.

Table 3
Whole-rock major and trace element compositions of the syenitic plutons.

Localities	Luku mine							Baicao mine				
Sample no.	LK11-33	LK11-47	LK11-49	LK11-50	LK11-55	LK11-57	LK11-58	BC12-15	BC12-16	BC12-18	BC12-19	BC12-22
Major oxides (wt.%)												
SiO_2	63.7	63.9	65.5	63.5	62.4	63.0	62.0	62.6	62.9	63.2	63.0	62.6
TiO_2	0.87	0.58	0.24	0.74	1.04	0.79	0.85	1.03	0.86	0.83	0.89	0.78
Al_2O_3	16.4	17.5	18.2	17.3	16.3	17.1	17.1	16.5	16.5	16.5	16.2	15.9
Fe_2O_3	4.47	3.83	1.53	3.99	5.09	4.17	3.99	5.08	4.95	4.82	5.25	5.82
MnO	0.16	0.12	0.06	0.15	0.21	0.13	0.14	0.19	0.18	0.19	0.19	0.21
MgO	0.62	0.45	0.35	0.54	0.90	0.75	0.67	0.72	0.66	0.59	0.75	0.77
CaO	0.88	0.64	0.33	0.68	1.49	1.21	1.19	1.16	1.09	0.96	1.16	1.23
Na_2O	6.47	7.18	7.02	6.84	6.72	7.24	7.18	6.92	6.93	7.19	7.07	6.73
K_2O	5.50	4.91	5.82	5.39	4.85	4.45	4.65	4.83	4.92	4.90	4.39	5.12
P_2O_5	0.11	0.04	0.01	0.04	0.18	0.19	0.16	0.16	0.14	0.05	0.15	0.13
LOI	0.34	0.31	0.37	0.27	0.31	0.44	0.52	0.29	0.28	0.22	0.45	0.20
ANK	0.99	1.02	1.02	1.01	1.00	1.02	1.01	0.99	0.98	0.96	0.99	0.96
ACNK	0.90	0.95	0.99	0.94	0.86	0.90	0.90	0.88	0.88	0.87	0.87	0.84
K_2O+Na_2O	12.0	12.1	12.8	12.2	11.6	11.7	11.8	11.8	11.9	12.1	11.5	11.9
Trace elements (ppm)												
Ti	5220	3480	1440	4440	6240	4740	5100	6180	5160	4980	5340	4680
Sc	9.62	8.49	8.57	7.90	8.63	9.35	9.77	10.40	10.40	9.18	10.00	10.60
V	4.13	8.11	4.07	15.3	17.9	8.36	7.46	6.76	6.38	5.36	7.19	7.72
Cr	4.34	6.51	3.84	3.00	4.97	2.97	2.59	3.88	2.68	4.72	3.00	3.70
Co	0.52	1.04	0.38	1.04	1.74	1.04	0.83	0.87	0.97	0.80	0.80	1.00
Ni	2.45	2.00	2.20	2.11	3.02	2.34	1.77	2.50	2.66	2.40	2.53	3.12
Cu	7.76	6.74	3.73	5.61	8.79	10.4	11.4	9.77	9.55	7.69	10.2	8.78
Zn	134	68.9	36.8	80.2	153	92.6	87.9	114	134	128	183	161
Ga	29.6	25.5	27.2	23.4	30.1	29.4	30.9	30.8	30.4	30.0	33.8	31.3
Rb	139	71.0	121	93.4	100	69.1	77.5	92.9	126	118	103	139
Sr	46.6	41.2	97.3	97.5	247	194	170	154	97.5	55.4	80.1	146
Y	21.7	5.90	5.08	7.00	69.8	25.7	25.4	21.1	26.8	31.0	68.7	28.0
Zr	441	24.4	87.4	78.1	638	124	206	139	209	266	499	152
Nb	89.2	9.40	30.4	39.2	156	45.5	53.9	77.5	83.1	94.0	154	83.4
Cs	0.59	0.34	0.57	0.25	0.60	0.76	1.35	0.92	0.85	0.36	0.94	0.32
Ba	763	246	1450	1300	1160	1860	2130	1970	1670	1080	1530	953
La	54.0	26.2	8.10	15.6	179	61.5	61.0	76.8	111	57.4	65.9	77.9
Ce	115	61.5	18.9	36.0	332	130	115	147	195	132	144	167

Table 3 *(continued)*

Localities	Luku mine							Baicao mine				
Sample no.	LK11-33	LK11-47	LK11-49	LK11-50	LK11-55	LK11-57	LK11-58	BC12-15	BC12-16	BC12-18	BC12-19	BC12-22
Trace elements (ppm)												
Pr	13.7	8.30	2.60	4.40	40.1	16.7	14.1	17.4	22.8	18.2	18.8	20.4
Nd	53.2	34.3	10.0	16.7	148	63.5	53.3	63.2	78.2	70.9	76.8	77.7
Sm	9.30	5.49	1.96	2.99	27.0	11.0	9.11	10.5	12.1	12.7	17.4	13.5
Eu	1.75	0.90	0.57	0.90	4.18	2.13	2.09	2.49	2.89	2.11	3.73	2.29
Gd	5.54	2.91	1.29	2.05	17.8	6.50	5.42	6.10	6.22	7.83	12.2	7.39
Tb	1.16	0.53	0.26	0.37	3.72	1.32	1.19	1.25	1.38	1.68	2.74	1.58
Dy	5.15	1.94	1.32	1.66	17.50	5.80	5.65	5.08	5.61	7.88	14.4	6.67
Ho	0.92	0.31	0.25	0.30	3.06	1.02	1.06	0.89	1.00	1.38	2.53	1.14
Er	2.83	0.79	0.74	0.89	8.49	2.78	3.12	2.67	2.96	3.79	6.44	3.20
Tm	0.36	0.08	0.11	0.12	0.98	0.32	0.39	0.33	0.36	0.48	0.83	0.40
Yb	2.74	0.55	0.83	0.92	6.07	1.91	2.62	2.36	2.55	3.36	4.86	2.74
Lu	0.42	0.10	0.14	0.17	0.84	0.28	0.38	0.37	0.40	0.54	0.71	0.46
Hf	11.6	0.83	2.76	2.16	14.5	3.21	5.58	4.08	5.18	8.07	11.3	4.06
Ta	5.33	0.76	2.42	1.91	15.9	3.01	2.87	4.00	4.05	9.03	8.34	4.45
Th	6.04	0.60	2.81	1.11	11.9	3.00	12.40	4.72	6.69	2.91	4.50	2.08
U	1.12	0.22	1.28	0.39	1.47	0.77	1.82	1.02	0.99	0.68	1.98	0.35
REE	288	150	52.1	90.0	859	330	300	358	469	351	440	410
Eu/Eu*	0.69	0.62	1.02	1.05	0.55	0.71	0.84	0.88	0.91	0.60	0.74	0.64

Table 4
Representative compositions of pyrochlore in the Nb–Ta-mineralized and Nb–Ta-poor syenitic dikes.

Occurrences	Nb–Ta-mineralized syenitic dikes							Nb–Ta-poor syenitic dikes			
Sample no.	LK11-1					LK-17		BC-4			
Points	1	1′	2	3	4	6	6′	7	8	9	10
Localities	Rim	Core				Core	Rim				
SiO_2	0.14	0.11	0.15	0.13	0.44	0.16	0.10	0.17	0.19	0.13	0.13
MgO	bdl	bdl	0.01	bdl	0	0	0.02	bdl	0.007	bdl	bdl
CaO	11.4	11.7	17.4	17.4	12.4	13.7	13.6	16.5	15.7	15.9	17.1
Na_2O	4.89	4.77	2.97	3.08	0.81	4.70	5.06	2.44	3.74	3.27	2.29
Nb_2O_5	47.7	46.8	49.1	49.1	51.3	48.1	51.0	47.4	44.8	43.9	45.5
Ta_2O_5	2.87	3.29	3.62	3.44	3.26	2.62	2.76	2.11	3.35	3.31	3.56
TiO_2	9.90	10.2	9.94	9.95	9.84	9.70	8.26	10.6	11.9	12.1	11.6
HfO_2	0.25	bdl	0.26	0.11	0.16	0.08	0.09	0.09	0.03	0.18	0.10
Ce_2O_3	6.76	7.01	2.88	3.83	4.67	2.99	3.00	5.66	4.10	3.56	4.04
UO_2	4.83	6.70	7.67	5.91	5.86	4.76	6.16	3.21	9.90	10.97	8.81
ThO_2	1.43	1.09	0.68	0.99	1.14	4.84	2.18	4.48	0.93	0.63	0.95
ZrO_2	0.10	0.13	0.02	0.11	bdl	0.03	0.05	0.02	0.01	0.07	0.02
Y_2O_3	0.52	0.40	0.22	0.32	0.32	0.67	0.52	0.33	0.56	0.46	0.51
F	2.68	2.51	2.49	2.40	1.62	3.17	3.45	2.18	2.24	2.15	1.91
Total	92.4	93.6	96.3	95.7	91.2	94.2	94.8	94.0	96.5	95.8	95.7
Si	0.036	0.027	0.036	0.031	0.110	0.039	0.024	0.040	0.046	0.033	0.031
Mg	bdl	bdl	0.002	bdl	0.001	0.001	0.006	bdl	0.002	bdl	bdl
Ca	3.081	3.143	4.451	4.452	3.328	3.638	3.581	4.322	4.064	4.174	4.445
Na	2.392	2.325	1.378	1.432	0.394	2.255	2.416	1.155	1.754	1.546	1.075
Nb	5.439	5.310	5.310	5.313	5.797	5.390	5.675	5.234	4.902	4.853	4.979
Ta	0.197	0.225	0.235	0.224	0.222	0.176	0.185	0.140	0.221	0.220	0.234
Ti	1.877	1.927	1.787	1.792	1.849	1.806	1.529	1.948	2.165	2.218	2.108
Hf	0.018	bdl	0.018	0.007	0.011	0.006	0.006	0.006	0.002	0.013	0.007
Ce	0.624	0.645	0.252	0.336	0.427	0.271	0.270	0.507	0.363	0.318	0.358
U	0.271	0.375	0.408	0.315	0.326	0.262	0.338	0.175	0.533	0.596	0.475
Th	0.082	0.062	0.037	0.054	0.065	0.273	0.122	0.249	0.051	0.035	0.053
Zr	0.012	0.016	0.002	0.013	bdl	0.004	0.007	0.003	0.002	0.008	0.002
Y	0.070	0.053	0.028	0.040	0.043	0.089	0.068	0.042	0.073	0.060	0.066
F	1.964	1.843	1.746	1.692	1.214	2.249	2.417	1.572	1.599	1.550	1.378

bdl: below detection limit.

Table 5
Representative compositions of titanite in the Nb–Ta-mineralized and Nb–Ta-poor syenitic dikes.

Occurrences	Nb–Ta-mineralized syenitic dikes								Nb–Ta-poor syenitic dikes				
Sample no.	LK11-1				LK-17				BC-2				
Points	1	2	3	4	5	6	7	8	1	2	3	5	6
SiO_2	29.3	29.2	28.9	28.7	29.5	28.7	28.7	28.6	29.5	29.7	29.3	29.8	29.4
MgO	bdl	bdl	bdl	bdl	bdl	bdl	bdl	bdl	0.02	bdl	0.02	0.03	0.03
CaO	23.8	22.9	22.8	22.3	20.7	19.9	21.2	20.0	28.3	28.4	26.2	28.9	25.6
Na_2O	2.31	2.44	2.44	2.09	2.88	3.08	3.01	3.20	0.65	0.75	1.22	0.43	1.31
K_2O	0.01	0.01	bdl	0.04	0.03	0.01	0.02	0.01	bdl	0.01	bdl	bdl	0.02
Nb_2O_5	2.12	2.57	1.78	3.34	3.53	3.86	3.22	2.69	0.75	0.61	2.82	0.41	2.17
Ta_2O_5	0.22	0.20	0.15	0.35	0.33	0.44	0.21	0.30	0.00	bdl	0.13	0.12	0.19
TiO_2	38.1	37.5	37.6	36.1	36.1	36.4	36.8	37.3	36.4	37.0	34.3	36.5	36.3
HfO_2	bdl	bdl	0.05	0.20	0.06	bdl	0.15	0.16	0.04	0.01	0.04	0.11	0.23
Ce_2O_3	1.61	1.96	1.43	2.24	2.03	2.55	2.04	2.25	0.54	0.41	1.30	0.46	1.70
UO_2	bdl	bdl	bdl	bdl	bdl	bdl	bdl	bdl	bdl	bdl	bdl	bdl	bdl
ThO_2	bdl	0.01	0.01	0.00	0.01	0.04	bdl	0.02	bdl	0.02	bdl	bdl	0.02
ZrO_2	0.16	0.49	0.32	0.22	0.24	0.06	0.52	0.21	0.45	0.46	0.82	0.60	0.49
Y_2O_3	0.41	0.85	0.62	0.84	0.71	0.89	0.42	0.71	0.05	0.02	0.18	bdl	0.19
F	0.51	0.32	0.78	0.22	0.18	0.42	0.30	0.50	0.58	0.60	0.42	0.45	0.58
Total	98.3	98.3	96.6	96.6	96.2	96.2	96.5	95.8	97.0	97.7	96.6	97.6	98.0
Si	4.762	4.767	4.780	4.786	4.897	4.808	4.771	4.792	4.839	4.822	4.871	4.856	4.823
Mg	bdl	bdl	bdl	bdl	bdl	bdl	bdl	bdl	0.004	bdl	0.006	0.007	0.008
Ca	4.154	3.997	4.054	3.982	3.692	3.566	3.783	3.589	4.974	4.952	4.666	5.047	4.488
Na	0.728	0.773	0.782	0.677	0.929	1.001	0.971	1.041	0.208	0.235	0.392	0.136	0.417
K	0.002	0.002	bdl	0.008	0.006	0.002	0.004	0.002	bdl	0.002	bdl	bdl	0.004
Nb	0.156	0.190	0.134	0.252	0.266	0.292	0.242	0.204	0.056	0.045	0.211	0.030	0.161
Ta	0.010	0.009	0.007	0.016	0.015	0.020	0.009	0.014	0.000	bdl	0.006	0.005	0.008
Ti	4.660	4.610	4.687	4.531	4.509	4.585	4.609	4.705	4.485	4.530	4.284	4.466	4.474
Hf	bdl	bdl	0.002	0.010	0.003	bdl	0.007	0.008	0.002	0.000	0.002	0.005	0.011
Ce	0.096	0.117	0.087	0.137	0.124	0.156	0.124	0.138	0.033	0.024	0.079	0.027	0.102
U	bdl	bdl	bdl	bdl	bdl	bdl	bdl	bdl	bdl	bdl	bdl	bdl	bdl
Th	bdl	0.000	0.000	0.000	0.001	0.002	bdl	0.001	bdl	0.001	bdl	bdl	0.001
Zr	0.013	0.039	0.026	0.018	0.020	0.005	0.042	0.017	0.036	0.037	0.066	0.047	0.039
Y	0.035	0.074	0.055	0.074	0.063	0.080	0.037	0.063	0.004	0.002	0.016	bdl	0.017
F	0.258	0.164	0.401	0.118	0.092	0.220	0.157	0.263	0.297	0.304	0.218	0.228	0.299

bdl: below detection limit.

Ta is likely related to the late-stage fluid–rock interaction in the highly evolved magma. We consider that the albitization of the Nb–Ta-mineralized syenitic dikes may be caused by the auto-metasomatism in a transitional, magmatic–hydrothermal stage. The evidence for such interaction is the epidote vein in the dikes (Fig. 5f); it is likely a result of the cations (K^+, Fe^{3+}, Mg^{2+}) that were released from early crystallized minerals (K-feldspar and aegirine) during albitization and combined with Na^+, Ca^{2+}, and OH^- released from hydrothermal fluids.

Experimental results indicate that Nb and Ta can be transported as Nb– and Ta–fluorine complexes with Na^+ in aqueous solutions (Wang et al., 1982). The Nb– and Ta–fluorine complexes would be decomposed when Na^+ is released from the complexes. We propose that large amounts of Nb– and Ta–fluorine complexes may be present in highly evolved, fluid-rich magmas in the late sage, and the resolution of the Nb– and Ta–fluorine complexes occurred when large amounts of albite crystallized because of intensive albitization in this stage. The decomposed Nb and Ta are compatible and finally entered the lattice of pyrochlore crystals. This model explains why Nb–Ta-bearing pyrochlore is always closely associated with albite and why the Nb–Ta-mineralized syenitic dikes are F-rich.

Table 6
Boron concentrations and B isotopic compositions of Nb–Ta-mineralized and Nb–Ta-poor syenitic dikes and syenitic plutons.

Sample no.	Occurrence	B (ppm)	$\delta^{11}B$ (‰)	$\pm 2\sigma$
LK1211	Nb–Ta-mineralized syenitic dikes	11.4	−16.40	0.03
LK1214		11.9	−15.79	0.03
BC-3		17.1	−14.54	0.04
BC-8		23.9	−17.95	0.04
BC-1	Nb–Ta-poor syenitic dikes	3.32	−11.96	0.03
BC-4		16.5	−12.84	0.04
BC11-15		9.09	−13.45	0.04
LK11-33	Syenitic plutons	9.43	−11.82	0.02
LK11-50		3.77	−12.45	0.03
BC1215		6.59	−10.96	0.03
BC1216		6.38	−10.02	0.02

7. Conclusions

The Nb–Ta-mineralized syenitic dikes in the Panxi region are products of highly evolved magma. Nb and Ta were decomposed from Nb– and Ta–fluorine complexes due to intensive albitization in the late stage and finally entered the lattice of pyrochlore crystals. The low and negative $\delta^{11}B$ of the rocks are consistent with the interaction of the rocks with magma-derived fluids in the late stage of the highly evolved magma.

Acknowledgment

Financial support for the study was obtained from a Chinese National “973” project (2011CB808903) and a GIGCAS 135 project Y234041001. Ma Yuxiao and Chen Wei are thanked for their guidance and sample collection in the field trip in the Panxi region.We are grateful to two anonymous reviewers and editor, Dr. F. Pirajno, for their

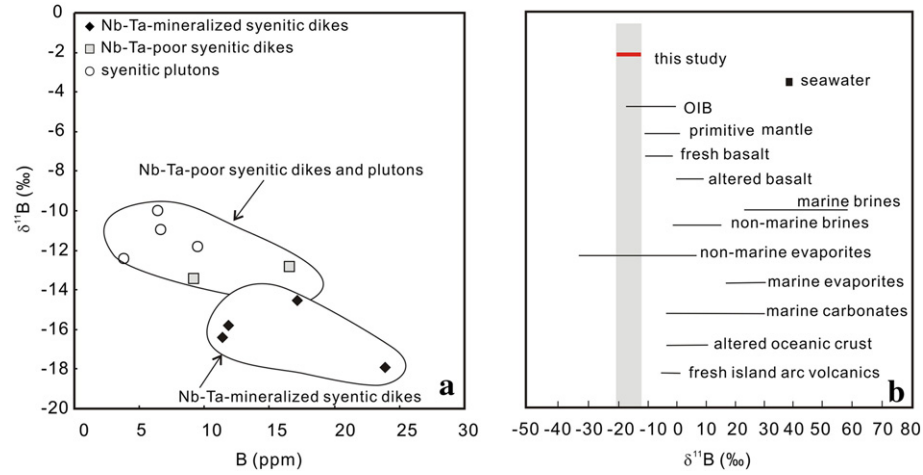

Fig. 10. A plot of B concentrations versus $\delta^{11}B$ values for the rocks in the Nb–Ta-mineralized and Nb–Ta-poor syenitic dikes and syenitic plutons (a), and a comparison of $\delta^{11}B$ values of the syenitic dikes in the Panxi region with different source rocks and fluids (b).
Data sources: OIB and primitive mantle from Chaussidon and Jambon (1994) and Chaussidon (1995), and other data from Palmer and Swihart (1996 and references therein).

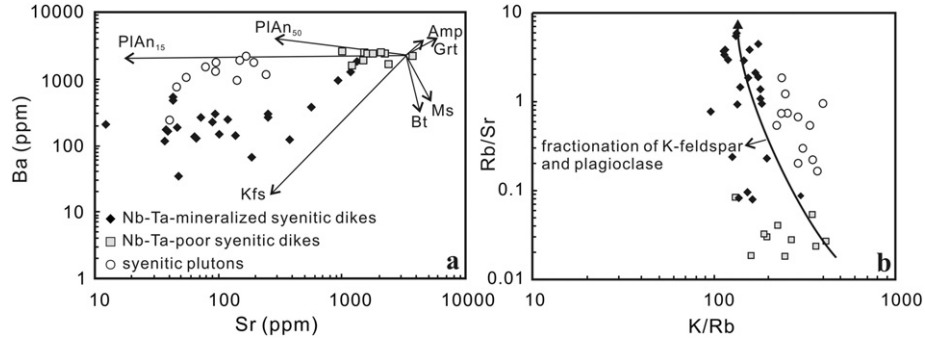

Fig. 11. Plot of Sr versus Ba (a) and Rb/Sr versus K/Ba (b) for the rocks of the Nb–Ta-mineralized and Nb–Ta-poor syenitic dikes and syenitic plutons.
Labeled vectors are after Janoušek et al. (2004) and Li et al. (2007).

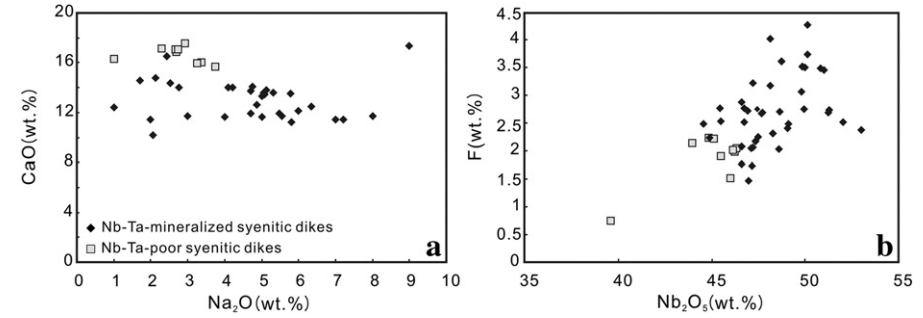

Fig. 12. Plots of Na_2O versus CaO (a) and Nb_2O_5 versus F (b) of pyrochlore crystals in the Nb–Ta-mineralized and Nb–Ta-poor syenitic dikes.

insights that helped improve this paper. This is a contribution No. IS-1955 from GIGCAS.

References

Bakker, J., Elburg, M.A., 2006. A magmatic–hydrothermal transition in Arkaroola (northern Flinders Ranges, South Australia): from diopside–titanite pegmatites to hematite–quartz growth. Contrib. Mineral. Petrol. 152, 541–569.
Barth, S., 1993. Boron isotope variations in nature: a synthesis. Geol. Rundsch. 82, 640–651.
Beus, A.A., Severon, V.A., Sitnin, A.A., Subbotin, R.D., 1962. Albitized and Greisenized Granites (Apogranites). Acad. Sci. Press, Moscow, p. 196.
Boily, M., Williams-Jones, A.E., 1994. The role of magmatic and hydrothermal processes in the chemical evolution of the Strange Lake plutonic complex, Québec-Labrador. Contrib. Depos. Petrol. 118, 33–47.
Brenan, J.M., Neroda, E., Lundstrom, C.C., Shaw, H.F., Ryerson, F.J., Phinney, D.L., 1998. Behavior of boron, beryllium, and lithium during melting and crystallization: constraints from mineral–melt partitioning experiments. Geochim. Cosmochim. Acta 62, 2129–2141.
Chaussidon, M., 1995. Isotope geochemistry of boron in mantle rocks, tektites and meteorites. C. R. Acad. Sci. Paris Ser. Iia 321, 455–472.
Chaussidon, M., Jambon, A., 1994. Boron content and isotopic composition of oceanic basalts: geochemical and cosmochemical implications. Earth Planet. Sci. Lett. 121, 277–291.
Chung, S.L., Jahn, B.M., 1995. Plume–lithosphere interaction in generation of the Emeishan flood basalts at the Permian–Triassic boundary. Geology 23, 889–892.
Deyhlea, A., Kop, A.J., 2005. The use and usefulness of boron isotopes in natural silicate–water systems. Phys. Chem. Earth 30, 1038–1046.
Dostal, J., Chatterjee, A.K., 2000. Contrasting behaviour of Nb/Ta and Zr/Hf ratios in a peraluminous granitic pluton (Nova Scotia, Canada). Chem. Geol. 163, 207–218.
Drake, M.J., Weill, D., 1975. Partition of Sr, Ba, Ca, Y, Eu^{2+}, Eu^{3+}, and other REE between plagioclase feldspar and magmatic liquid: an experimental study. Geochim. Cosmochim. Acta 39, 689–712.

Garda, G.M., Trumbull, R.B., Beljavskis, P., Wiedenbeck, M., 2009. Boron isotope composition of tourmalinite and vein tourmalines associated with gold mineralization, Serra do Itaberaba Group, central Ribeira Belt, SE Brazil. Chem. Geol. 264, 207–220.
Hadj-Kaddour, Z., Liégeois, J.P., Demaiffe, D., Caby, R., 1998. The alkaline–peralkaline granitic post-collisional Tin Zebane dyke swarm (PanAfrican shield, Algeria): Prevalent mantle signature and late agpaitic differentiation. Lithos 45, 223–243.
He, J.L., 2004. Ore-forming geological conditions and prospecting potential for Nb–Ta mineral deposits in Panzhihua–Xichang Region, Sichuan. Acta Geol. SiChuan 24, 206–211 (in Chinese with English abstract).
Hershry, J.P., Fernandez, M., Milne, P.J., et al., 1986. The ionization of boric acid in Nacl, Na–Ca–Cl and Na–Mg–Cl solution at 25 °C. Geochim. Cosmochim. Acta 50, 145–148.
Hervig, R.L., Moore, G.M., Williams, L.B., Peacock, S.M., Holloway, J.R., Roggensack, K., 2002. Isotopic and elemental partitioning of boron between hydrous fluid and silicate melt. Am. Mineral. 87, 769–774.
Janoušek, V., Finger, F., Roberts, M., Frýda, J., Pin, C., Dolejš, D., 2004. Deciphering the petrogenesis of deeply buried granites: whole-rock geochemical constraints on the origin of largely undepleted granulites from the Moldanubian Zone of the Bohemian Massif. Trans. R. Soc. Edinb. Earth Sci. 95, 141–159.
Jiang, S.Y., Palmer, M.R., Slack, J.F., Shaw, D.R., 1998. Paragenesis and chemistry of multistage tourmaline formation in the Sullivan Pb–Zn–Ag deposit, British Columbia. Econ. Geol. 93, 47–67.
Jiang, S.Y., Palmer, M.R., Slack, J.F., Shaw, D.R., 1999. Boron isotope systematics of tourmaline formation at the Sullivan Pb–Zn–Ag deposit, British Columbia. Chem. Geol. 158, 131–144.
Kakihana, H., Kotaka, M., Satoh, S., Nomura, M., Okamoto, M., 1977. Fundamental studies on ion exchange separation of boron isotopes. Bull. Chem. Soc. Jpn. 50, 158–163.
Kakihana, H., Nomura, M., Kanzaki, T., Ozawa, T., Okamoto, M., 1982. Boron isotopic composition of fumarolic condensates from some volcanoes in Japanese island arcs. Abstracts-International Conference on Geochronology, Cosmochronology. Isotope Geology 5, p. 176.
Kaliwoda, M., Marschall, H.R., Marks, M.A.W., Luding, T., Altherr, R., Markl, G., 2011. Boron and boron isotope systematics in the peralkaline Ilímaussaq intrusion (South Greenland) and its granitic country rocks: a record of magmatic and hydrothermal processes. Lithos 125, 51–64.
Kempe, U., Gotze, J., Dandar, S., Habermann, D., 1999. Magmatic and metasomatic processes during formation of the Nb–Zr–REE deposits Khaldzan Buregte and Tsakhir (Mongolian Altai): indications from a combined CL–SEM study. Mineral. Mag. 63, 165–177.
Klemme, S., Blundy, J.D., Wood, B.J., 2002. Experimental constraints on major and trace element partitioning during partial melting of eclogite. Geochim. Cosmochim. Acta 66, 3109–3123.
Kovalenko, V.I., Tasryeva, G.M., Goreglyad, A.V., Yarmolyuk, V.V., Troitsky, V.A., 1995. The peralkaline granite-related Khaldzan-Buregtey rare metal (Zr, Nb, REE) deposit, Western Mongolia. Econ. Geol. 90, 530–547.
Leeman, W.P., Sisson, V.B., 1996. Geochemistry of boron and its implications for crustal and mantle processes. In: Grew, E.S., Anovitz, L.M. (Eds.), Boron: Mineralogy, Petrology and GeochemistryReviews in Mineralogy. Mineralogical Society of America, pp. 645–708.
Li, X.H., Li, Z.X., Li, W.X., Liu, Y., Yuan, C., Wei, G.J., Qi, C.S., 2007. U–Pb zircon, geochemical and Sr–Nd–Hf isotopic constraints on age and origin of Jurassic I- and A-type granites from central Guangdong, SE China: a major igneous event in response to foundering of a subducted flat-slab? Lithos 96, 186–204.
Li, W.Y., Niu, Y.L., Zhang, Z.W., Zhang, M.J., Gao, Y.B., Hu, P.Q., Zhang, J.W., Tan, W.T., Jiang, H.B., 2012. Geodynamic setting and further exploration of magmatism-related mineralization concentrated in the late Paleozoic in the Northern Xinjiang Autonomous Region. Earth Sci. Front. 19, 041–050.
Ma, Y.X., Ji, X.T., Li, J.C., Huang, M., Min, Z.Z., 2003. Mineral resources of Panzhihua, Sichuan Province, SW China. Chengdu University of Technology, p. 275.
Markl, G., Baumgartner, L., 2002. pH changes in peralkaline late-magmatic fluids. Contrib. Mineral. Petrol. 144, 331–346.
Oi, T., Nomura, M., Ossaka, T., et al., 1989. Boron isotopic composition of some boron Minerals. Geochim. Cosmochim. Acta 53, 3189–3195.
Palmer, M.R., Slack, J.F., 1989. Boron isotopic composition of tourmaline from massive sulfide deposits and tommalinites. Contrib. Mineral. Petrol. 103, 434–451.
Palmer, M.R., Swihart, G.H., 1996. Boron isotope geochemistry: an overview. Rev. Mineral. 33, 709–744.
Pang, K.N., Li, C., Zhou, M.F., Ripley, E.M., 2009. Mineral compositional constraints on petrogenesis and oxide ore genesis of the late Permian Panzhihua layered gabbroic intrusion, SW China. Lithos 110, 199–214.
Qi, L., Hu, J., Gregoire, D.C., 2000. Determination of trace elements in granites by inductively coupled plasma mass spectrometry. Talanta 51, 507–513.
Shellnutt, J.G., Iizuka, Y., 2012. Oxidation zonation within the Emeishan large igneous province: evidence from mantle-derived syenitic plutons. J. Asian Earth Sci. 31–40.
Shellnutt, J.G., Zhou, M.F., 2007. Permian peralkaline, peraluminous and metaluminous A-type granites in the Panxi district, SW China: their relationship to the Emeishan mantle plume. Chem. Geol. 243, 286–316.
Shellnutt, J.G., Zhou, M.F., Yan, D.P., Wang, Y., 2008. Longevity of the Permian Emeishan mantle plume (SW China): 1 Ma, 8 Ma or 18 Ma? Geol. Mag. 145, 373–388.
Shellnutt, J.G., Zhou, M.F., Zellmer, G.F., 2009a. The role of Fe–Ti oxide crystallization in the formation of A-type granitoids with implications for the Daly gap: an example from the Permian Baima complex, SW China. Chem. Geol. 259, 204–217.
Shellnutt, J.G., Wang, C.Y., Zhou, M.F., Yang, Y.H., 2009b. Zircon Lu–Hf isotopic compositions of metaluminous and peralkaline A-type granitic plutons of the Emeishan large igneous province (SW China): constraints on the mantle source. J. Asian Earth Sci. 35, 45–55.
Sichuan Bureau of Geology, 403 geological team, 1965. The Lecture of Detail Exploration About Luku Nb, Ta Deposit in the Panxi Region (Internal Report).
Sichuan Bureau of Geology, Xichang geological team, 1962. The Lecture of Detail Exploration about Baicao Nb, Ta Deposit in the Panxi Region (Internal Report).
Slack, J.F., 1996. Tourmaline associations with hydrothermal ore deposits. In: Grew, E.S., Anovitz, L.M. (Eds.), Boron: Mineralogy, Petrology and GeochemistryReviews in Mineralogy. Mineralogical Society of America, pp. 559–644.
Slack, J.F., Palmer, M.R., Stevens, B.J., Barnes, R.C., 1993. Origin and significance of tourmaline-rich rocks in the Broken Hill District, Australia. Econ. Geol. 88, 505–541.
Sun, S.S., McDonough, 1989a. Chemical and isotopic systematics of oceanic basalts: implications for mantle composition and processes. In: Saunders, A.D., Norry, M.J. (Eds.), Magmatism in the Ocean Basin, Geological Society Special Publication. Blackwell Scientific Publications 42, pp. 313–346.
Sun, S.S., McDonough, W.F., 1989b. Chemical and isotopic systematics of oceanic basalts: implications for mantle composition and processes. In: Saunders, S.D., Norry, M.J. (Eds.), Magmatism in Ocean Basins. Geol. Soc. London. Spec. Pub. 42, pp. 313–345.
Tonarini, S., Forte, C., Petrini, R., Ferrara, G., 2003. Melt/biotite $^{11}B/^{10}B$ isotopic fractionation and the boron local environment in the structure of volcanic glasses. Geochim. Cosmochim. Acta 67, 1863–1873.
Wang, C.Y., Zhou, M.F., 2006. Genesis of the Permian Baimazhai magmatic Ni–Cu–(PGE) sulfide deposit, Yunnan, SW China. Miner. Depos. 41, 771–783.
Wang, Y.R., Li, J.T., Lu, J.L., Fan, W.L., 1982. Geochemical mechanism of Nb-, Ta-mineralization during the late stage of granite crystallization. Geochemistry 1, 175–185.
Wang, C.Y., Zhou, M.F., Qi, L., 2010. Origin of extremely PGE-rich mafic magma system: an example from the Jinbaoshan ultramafic sill, Emeishan large igneous province, SW China. Lithos 119, 147–161.
Wang, F.L., Zhao, T.P., Chen, T.W., Wang, Y., 2013. Zircon U–Pb ages and Lu–Hf isotopic compositions of the Nb–Ta–Zr-bearing syenitic dikes in the Emeishan large igneous province. Acta Petrol. Sin. 29, 3519–3532 (in Chinese with English abstract).
Wei, G.J., Wei, J.X., Liu, Y., Ke, T., Ren, Z.Y., Ma, J.L., Xu, Y.G., 2013. Measurement on high-precision boron isotope of silicate materials by a single column purification method and MC-ICP-MS. J. Anal. At. Spectrom. 28, 606–612.
Weill, D., Drake, M.J., 1973. Europium anomaly in plagioclase feldspar: experimental results and semiquantitative model. Science 180, 1059–1060.
Werding, G., Schreyer, W., 2002. Experimental studies on borosilicates and selected borates. In: Grew, E.S., Anovitz, L.M. (Eds.), Boron—Mineralogy, Petrology and GeochemistryReviews in Mineralogy 33. Mineralogical Society of America, pp. 117–163.
Xiao, L., Pirajno, F., He, Q., 2007. A preliminary discussion on large igneous provinces and associated ore deposits. Geol. J. China Univ. 13, 148–160.
Xing, C.M., Wang, C.Y., Zhang, M.J., 2012. Volatile and C – H – O isotopic compositions of giant Fe–Ti–V oxide deposits in the Panxi region and their implications for the sources of volatiles and the origin of Fe–Ti oxide ores. Sci. China Earth Sci. 55, 1782–1795.
Xu, Y.G., Chung, S.L., Jahn, B.M., Wu, G.Y., 2001. Petrologic and geochemical constraints on the petrogenesis of Permian Triassic Emeishan flood basalts in southwestern China. Lithos 58, 145–168.
Xu, Y.G., Luo, Z.Y., Huang, X.L., He, B., Xiao, L., Xie, L.W., Shi, Y.R., 2008. Zircon U–Pb and Hf isotope constraints on crustal melting associated with the Emeishan mantle plume. Geochim. Cosmochim. Acta 72, 3084–3104.
Yan, D.P., Zhou, M.F., Song, H.L., Wang, X.W., Malpas, J., 2003. Origin and tectonic significance of a Mesozoic multi layer over thrust system within the Yangtze Block (South China). Tectonophysics 361, 239–254.
Yang, W.B., Niu, H.C., Shan, Q., Luo, Y., Yu, X.Y., Qiu, Y.Z., 2009. Ore-forming mechanism of the Baerzhe super-large rare and earth elements deposit. Acta Petrol. Sin. 25, 2924–2932.
Yin, L., Pollard, P.J., Hu, S.X., Taylor, R.G., 1995. Geologic and geochemical characteristics of the Yichun Ta–Nb–Li deposit, Jiangxi Province, South China. Econ. Geol. 90, 577–585.
Zhong, H., Yao, Y., Hu, S.F., Zhou, X.H., Liu, B.G., Sun, M., Zhou, M.F., Viljoen, M.J., 2003. Trace-element and Sr–Nd isotopic geochemistry of the PGE-bearing Hongge layered intrusion, southwestern China. Int. Geol. Rev. 45, 371–382.
Zhong, H., Zhu, W.G., Chu, Z.Y., He, D.F., Song, X.Y., 2007. SHRIMP U–Pb zircon geochronology, geochemistry, and Nd–Sr isotopic study of contrasting granites in the Emeishan large igneous province, SW China. Chem. Geol. 236, 112–133.
Zhong, H., Zhu, W.G., Hu, R.Z., Xie, L.W., He, D.F., Liu, F., Chu, Z.Y., 2009. Zircon U–Pb age and Sr–Nd–Hf isotope geochemistry of the Panzhihua A-type syenitic intrusion in the Emeishan large igneous province, southwest China and implications for growth of juvenile crust. Lithos 110, 109–128.
Zhong, H., Qi, L., Hu, R.Z., Zhou, M.F., Gou, T.Z., Zhu, W.G., Liu, B.G., Chu, Z.Y., 2011. Rhenium–osmium isotope and platinum-group elements in the Xinjie layered intrusion, SW China: implications for source mantle composition, mantle evolution, PGE fractionation and mineralization. Geochim. Cosmochim. Acta 75, 1621–1641.
Zhou, M.F., Malpas, J., Song, X.Y., Robinson, P.T., Sun, M., Kennedy, A.K., Lesher, C.M., Keays, R.R., 2002a. A temporal link between the Emeishan large igneous province (SW China) and the end-Guadalupian mass extinction. Earth Planet. Sci. Lett. 196, 113–122.
Zhou, M.F., Yan, D.P., Kennedy, A.K., Li, Y., Ding, J., 2002b. SHRIMP U–Pb zircon geochronological and geochemical evidence for Neoproterozoic arc-magmatism along the western margin of the Yangtze block, South China. Earth Planet. Sci. Lett. 196, 51–67.
Zhou, M.F., Robinson, P.T., Lesher, C.M., Keays, R.R., Zhang, C.J., Malpas, J., 2005. Geochemistry, petrogenesis and metallogenesis of the Panzhihua gabbroic layered intrusion and associated Fe–Ti–V oxide deposits, Sichuan Province, SW China. J. Petrol. 46, 2253–2280.
Zhou, M.F., Arndtb, N.T., Malpas, J., Wang, C.Y., Kennedy, A.K., 2008. Two magma series and associated ore deposit types in the Permian Emeishan large igneous province, SW China. Lithos 103, 352–368.